Supplementary Materials for

Chronic Traumatic Encephalopathy in Blast-Exposed Military Veterans and a Blast Neurotrauma Mouse Model

Lee E. Goldstein,* Andrew M. Fisher, Chad A. Tagge, Xiao-Lei Zhang, Libor Velisek, John A. Sullivan, Chirag Upreti, Jonathan M. Kracht, Maria Ericsson, Mark W. Wojnarowicz, Cezar J. Goletiani, Giorgi M. Maglakelidze, Noel Casey, Juliet A. Moncaster, Olga Minaeva, Robert D. Moir, Christopher J. Nowinski, Robert A. Stern, Robert C. Cantu, James Geiling, Jan K. Blusztajn, Benjamin L. Wolozin, Tsuneya Ikezu, Thor D. Stein, Andrew E. Budson, Neil W. Kowall, David Chargin, Andre Sharon, Sudad Saman, Garth F. Hall, William C. Moss, Robin O. Cleveland, Rudolph E. Tanzi, Patric K. Stanton, Ann C. McKee*

*To whom correspondence should be addressed. E-mail: lgold@bu.edu (L.E.G.); amckee@bu.edu (A.C.M)

This PDF file includes:

MATERIALS & METHODS

Human Subjects. The brain and spinal cord of 12 human subjects (male military veterans, ages 22 to 45 years, mean 32.3 years, with histories of explosive blast and/or concussive injury 1 to 6 years before death, n = 4; male athletes with histories of repetitive concussive injury, including 3 amateur American football players and a professional wrestler, ages 17 to 27 years, mean 20.8 years, n = 4; male normal controls, ages 18 to 24 years, mean 20.5 years, without known blast exposure, trauma history, or neurological disease, n = 4) were procured through the Boston University Alzheimer's Disease Center and Center for the Study of Traumatic Encephalopathy at Boston University School of Medicine. Blast exposure, trauma history, and neurological status at the time of death were determined through review of medical records and interviews with next of kin. Ethical permission to conduct this investigation was approved by Institutional Review Board at Boston University School of Medicine. The study conforms to institutional regulatory guidelines and principles of human subject protection in the Declaration of Helsinki.

Animal Subjects. Adult wildtype C57BL/6 male mice were purchased from Charles River Laboratories (Wilmington, MA) and group housed at the Laboratory Animal Science Center, Boston University School of Medicine, Boston, MA. All animal experiments utilized 2.5-month-old mice at the time of blast exposure and included 8 to 10 mice per group. Mice were provided with standard mouse chow and water *ad libitum*. Ambient temperature was controlled at 20-22 $^{\circ}$C with 12-hour light-dark cycles. Animal housing and experimental use were conducted in accordance with Association for Assessment and Accreditation of Laboratory Animal Care guidelines, in compliance with the Animal Welfare Act and other federal statutes and regulations relating to animals and experiments involving animals, and adherence to principles in the National Research Council Guide for the Care and Use of Laboratory Animals. All studies were approved by Institutional Animal Care and Use Committees at Boston University School of Medicine and New York Medical College.

Histopathology. Processing of human brains followed established procedures and protocols at the Boston University Alzheimer's Disease Center, Boston, MA, and included comprehensive neuropathological analysis of all neurodegenerative conditions as previously described (*1*). Human brain and spinal cord specimens were received as fixed tissue in formalin after processing by medical

examiners. Paraffin-embedded sections from at least 15 brain regions were stained with Luxol fast blue, hematoxylin and eosin, and Bielschowsky silver stain. Sections evaluated by immunohistochemistry utilized a battery of primary antibodies (table S1), chromogen visualization (Vectastain Elite ABC Kit, Vector Labs, Burlingame, CA), and cresyl violet counterstaining as previously described (*2, 3*). For histological experiments involving mice, animals were euthanized by CO_2 asphyxiation according to IACUC-approved protocol followed by transcardial gravity perfusion with phosphate-buffered saline (PBS, Sigma-Aldrich, St Louis, MO). Brains were rapidly removed from the calvarium and placed in 10% neutral buffered formalin for 2 hours, then transferred to PBS. Coronal slabs (2 mm) were obtained by block sectioning, fixed in 4% paraformaldehyde for 2 hours, embedded in a single paraffin block, and serially sectioned at 10 μm. Sections were processed for immunohistochemistry with a battery of primary antibodies (table S1) and visualized by Vectastain Elite ABC Kit (Vector Labs, Burlingame, CA). Slides were developed according to manufacturer's instructions for exactly the same incubation time and counterstained with hematoxylin. For double immunostained sections, tissue was blocked with avidin and biotin before primary antibody incubation and visualized with DAB and aminoethylcarbazole according to manufacturer's instructions (Vector Laboratories, Burlingame, CA, USA). Bielschowsky silver stain was performed using 20% $AgNO_3$ titrated with ammonia and developed with HNO_3 and citric acid and unbuffered formalin.

Electron Microscopy. Small pieces (1-2 mm cubes) of harvested brain were fixed in 2.5% glutaraldehyde with 2.5% paraformaldehyde in 0.1M sodium cacodylate buffer (pH 7.4) overnight at room temperature, washed in 0.1M cacodylate buffer, postfixed with 1% osmium tetroxide (OsO_4) with 1.5% potassium ferrocyanide ($KFeCN_6$) for 1 hour, then washed in water. The specimens were then incubated in 1% aqueous uranyl acetate for 1hr, washed, and sequentially dehydrated in increasing grades of alcohol (10 min each in 50%, 70%, 90%, 100%, 100%). Samples were treated in propylene oxide for 1 hr and infiltrated overnight in a 1:1 mixture of propylene oxide and TAAB Epon (Marivac Canada Inc., St. Laurent, Canada) and polymerized at 60 $^{\circ}$C for 48 hrs. Ultrathin sections (60 nm) were cut on a Reichert Ultracut-S microtome, placed on copper grids, stained with lead citrate or uranyl acetate, and examined using a Tecnai-G2 Spirit BioTWIN electron microscope. Images were acquired with an AMT 2K CCD camera.

Murine Blast Neurotrauma Model. A compressed gas-driven shock tube (25 cm diameter; 5.3 m tube length; fig. S2) developed in collaboration with the Fraunhofer Center for Manufacturing Innovation at Boston University, Boston, MA, and installed at the Murine Neurotrauma Laboratory, Boston University School of Medicine, Boston, MA was used to deliver highly-reproducible sublethal blast shock waves relevant to human blast injury (fig. S2-6; tables S2, S3). Adult wildtype C57BL/6 male mice (Charles River Laboratories, Wilmington, MA) at 2.5-months-of-age were anesthetized with ketamine (75 mg/kg, i.p.), xylazine (4.3 mg/kg, i.p.), and buprenorphine (0.2 mg/kg, s.c.), secured in the prone position with a wire mesh holder, and inserted into a custom-fabricated restraint system that protected the thorax. The assembly was then fixed to an internal frame inside the shock tube with the unprotected head positioned exactly 0.56 m from the exit of the shock tube and 4.06 m from the blast origin (fig. S2). In order to model conditions relevant to human blast exposure conditions, the head and neck were free to allow flexion, extension, and rotation of the cervical spine in the sagittal and horizontal planes of motion. We empirically determined the maximum burst pressure (303 $\pm$ 9 kPag) and corresponding blast parameters compatible with 100% survival with no gross motor abnormalities 24 hours following blast exposure (table S2). Anesthetized mice were exposed to a single sublethal shock tube blast (table S2) or sham blast, removed from the apparatus, and monitored until recovery of gross locomotor function and exploratory activity. Mice were then transferred to their home cage.

Blast Comparators. Experimental shock tube blast parameters (i.e., peak static pressure amplitude, duration, and impulse) used in this study closely approximated characteristics of explosive blast produced by detonation of 5.8 kg of 2,4,6-trinitrotoluene (TNT) or 4.5 kg of Composition C-4 explosive measured at a standoff distance of 5.53 m (table S3) analyzed using the Conventional Weapons Effects Program (ConWep) (*44*). For comparison, an improvised explosive device (IED) commonly encountered by U.S. military personnel utilizes a 120 mm mortar round equivalent to 4.53 kg of TNT (1st Infantry Division Soldier's Handbook to Iraq, U.S. Army, at weblink: http://www.gwu.edu/~nsarchiv/IMG/soldiershandbookiraq.pdf accessed January 2, 2012 (L.E.G.). The blast exposure utilized in this study was comparable to experimental conditions in recent studies utilizing a shock tube (*4, 5*) or detonated explosives (*6*) to model moderate intensity blast exposure relevant to the military.

Static and Reflected Free-Field Pressure Measurements. Assessment of static (side-on) and reflected (face-on) free-field pressure (FFP) during blast exposure was assessed by two piezoelectric pressure sensors (Model HM102A15, PCB Piezotronics Inc., Depew, NY, USA) placed in the shock tube at the same axial distance as the head of the mouse. One sensor was flushed-mounted inside the shock tube and secured in a static pressure (side-on) orientation relative to the blast shock wave. The second transducer was positioned with the detector facing into the shock tube in a reflected pressure (face-on) orientation relative to the blast shock wave. With respect to the reflected pressure sensor, the measured pressure magnitude does not capture the total pressure (i.e., stagnation pressure) of the blast wave as a consequence of the small size and geometry of the sensor system relative to the blast wave produced by our shock tube system. However, the reflected pressure transducer was comparable in size to the mouse head and thus recorded relevant pressure incident to the head during blast exposure. Pressure signals in both orientations were processed through a PCB signal conditioner (Model 482C05, PCB Piezotronics Inc., Depew, NY, USA) and recorded at a frequency of 2 MHz using a digital oscilloscope (640Zi Waverunner; LeCroy, Chestnut Ridge, NY). Voltages were converted to pressure using calibration data.

Intracranial Pressure Measurements. Intracranial pressure (ICP) measurements were conducted with a broad-bandwidth piezoelectric needle hydrophone (NP10-3; DAPCO Industries Inc., Oak Creek, WI) with a 0.6 mm diameter active element sheathed in a standard #19 gauge hypodermic needle (length, 75 mm; o.d., 1 mm). Pressure transducer sensitivity was flat to within ±3 dB for frequencies ranging from 1 Hz to 170 kHz. The needle hydrophone was inserted into the hippocampus (-3.00 mm caudal to the bregma suture, +3.50 mm lateral to the sagittal suture, +2.00 mm ventral to skull surface according to the atlas of Franklin and Paxinos *The Mouse Brain in Stereotaxic Coordinates*, 3rd Ed., Elsevier Academic Press, Boston, 2008. For ICP measurements, the head was secured in place to prevent intracranial displacement during blast exposure. ICP piezoelectric voltage signals were recorded by a digital oscilloscope (640Zi Waverunner; LeCroy, Chestnut Ridge, NY) converted to pressure using calibration data derived from substitution experiments with calibrated transducers over a frequency range up to 2 MHz. Post-acquisition processing was performed with Matlab 2009 software (MathWorks, Natick, MA, USA).

High-Speed Videography and Kinematic Analysis. High-speed videography was conducted with a FASTCAM SA5 camera and software (Photron USA Inc., San Diego, CA) operated at a 10 μs frame capture rate (100 kHz). Initial post-acquisition analysis of individual frames was conducted using ImageJ software (NIH, Bethesda, MD). All subsequent processing was carried out in Matlab (MathWorks, Natick, MA). Angular rotation of the head was calculated by assuming a central pivot point between the scapulae (fig. S2B). Cartesian motion of the head was calculated by tracking a paintmarked nose spot.

Head Fixation. Head fixation was accomplished using two miniature nylon cable ties with minimal face-on cross-sectional area. Prior to immobilization, the head was securely positioned on a rigid bite bar fixed to the in-tube restraint. The head was immobilized by positioning one band across the rostral aspect of the skull proximal to the incisor. The second band was placed immediately posterior to the caudalmost aspect of the skull. Neither band obstructed the oncoming blast shock wave (see figure, *right*). Care was taken to avoid airway compromise. Thoracic protection was provided as described above. This immobilization procedure prohibited head displacement in all three Cartesian planes of motion during experimental blast.

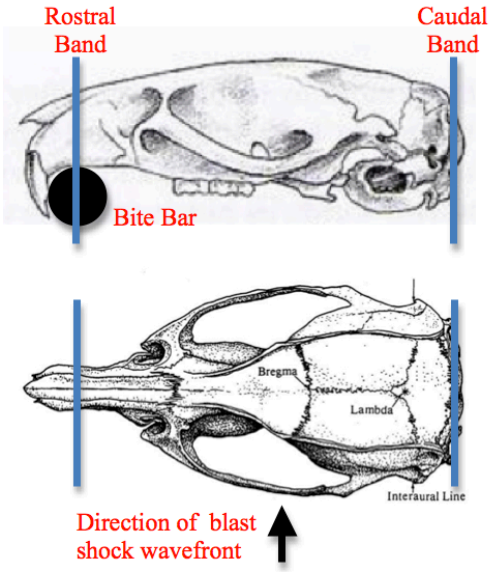

Mouse Hippocampus Slice Electrophysiology. Mice were decapitated under deep isoflurane anesthesia and the brains quickly removed, hemisected, and blocked with a vibratome (DTK1000, Ted Pella, Co., Redding, CA) at a thickness of 350 μm. The tissue block was glued with cyanoacrylate adhesive to a stage immersed in ice-cold, oxygenated artificial cerebrospinal fluid (aCSF; NaCl, 126 mM; KCl, 3 mM; NaH_2PO_4,1.25 mM; MgCl, 1.3 mM; $CaCl_2$, 2.5 mM; $NaHCO_3$, 26 mM; glucose, 10 mM; saturated with 95% O_2 and 5% CO_2) maintained at 2-4 °C, then placed in a conditioning chamber containing aCSF at room temperature for at least 1 hr before transfer to an interface chamber maintained at 32°C for recording. Slices were perfused with aCSF during experiments. Experimental drugs were bath applied in the perfusate. For studies of Schaffer Collateral-CA1 synaptic transmission and plasticity, low resistance recording electrodes were pulled

with a Flaming/Brown Micropipette puller (Model P-97, Sutter Instrument, Novato, CA, USA) using thin-walled borosilicate glass (1-2 MΩ with aCSF; A-M Systems, Sequim, WA), and inserted into the *stratum radiatum* of the hippocampus CA1 field to record field excitatory post-synaptic potentials (fEPSPs). A bipolar stainless steel stimulating electrode was placed in Schaffer collateral-commissural fibers the *stratum radiatum*, and current pulses were applied with stimulus intensity adjusted to evoke approximately 50% of maximal fEPSPs (50 pA to 100 pA; 100 *μ*s duration) at 30 s intervals. Electrical stimulation was delivered by an ISO-Flex isolator controlled by a Master eight-pulse generator (AMPI, Jerusalem, Israel) triggered by a Multiclamp 700B amplifier (Molecular Devices, Sunnyvale, CA), and signals were digitized and recorded using the Multiclamp 700B. fEPSP slope was measured by linear interpolation from 20-80% of maximum negative deflection, and slopes confirmed to be stable $\pm$10% for at least 15 min. Data were analyzed using Clampfit (Version 9, Molecular Devices, Sunnyvale, CA) on an IBM-compatible personal computer. Evoked fEPSPs (50% of maximum amplitude, 2-4 mV) were recorded in the apical dendritic field in *stratum radiatum* for a stable baseline period of at least 30 min and evoked by single square pulses (10-100 *μ*A, 150 *μ*s) applied at 30 s intervals from a bipolar stainless-steel stimulating electrode (FHC, Bowdoin, ME). The high-frequency stimulus (HFS) paradigm for induction of homosynaptic LTP consisted of three theta burst trains, each train consisting of 10 bursts of 5 pulses each with a burst frequency of 100Hz with interburst interval of 200 ms applied at 120 s intervals. For measurement of axonal conduction velocity, two extracellular recording electrodes were placed in CA1 *stratum alveus* approximately 200 *μ*m apart, and a bipolar stimulating electrode placed 100 *μ*m away from the nearest of the two recording electrodes to antidromically activate CA1 pyramidal neuron axons coursing through the *stratum alveus*. The latency differences of the peak negativity between the two recording electrodes and the spatial distance were used to calculate axonal conduction velocity for each slice.

Assessment of Hippocampal-Dependent Learning and Memory. Neurobehavioral assessment was performed using an open-field test and Barnes maze (Med-Associates, Inc., St. Albans, VT, USA). Open-field testing to assess baseline locomotor functioning (average velocity), exploratory activity (total distance), and thigmotaxis (number of central zone entries) was performed by placing each animal subject in the middle of a 42.5 cm x 42.5 cm open arena and monitoring movement for 10 min using a 3D infrared diode motion detector system (Any-Maze, Stoelting Co., Inc., Wood Dale, IL). Barnes maze evaluation (*7*) was conducted using a 20-box apparatus with 900 lux surface light

intensity. Animal subjects were familiarized with the test apparatus by placement on the platform and gentle guidance to the escape box. Training sessions were conducted across four training trials per day for four days. The order of testing of individual subjects was the same throughout daily sessions, but randomized across the four test days for a total of 16 trials. To initiate testing, a single mouse was placed in the start box in the middle of the maze and released. Test subjects were evaluated while locating a single escape box placed at a constant position. Spatial learning was assisted by distant visual cues that remained constant during across test sessions. Movement was tracked and recorded electronically. Latency to find the escape box, trajectory velocity to the escape box, and total trajectory distance was assessed and recorded daily. Memory retrieval was evaluated by replacing the escape box with a blank box 24 hours after the last training session. Memory retrieval was assessed by electronically recording the number of nose pokes into the blank box as a percentage of total nose pokes.

Quantitative Assessment of Phosphorylated and Total Tau Protein. For immunoblot analysis, left and right hemisected brain samples were obtained from PBS-perfused mice 2 weeks after exposure to a single shock tube blast (n = 6 mice) or sham blast (n = 6 mice). Snap frozen hemisected brain specimens were thawed and resuspended in 0.7 ml protease-phosphatase inhibitor buffer as previously described (*8*). Equal volumes of homogenized samples were subjected to standard polyacrylamide gel electrophoresis in duplicate and immunoblotted with monoclonal antibody AT270 (Innogenetics Inc., Alpharetta, GA, USA) directed against tau protein phosphorylated at threonine-181 (pT181), monoclonal antibody CP-13 (Dr. Peter Davies, Albert Einstein College of Medicine, Manhasset, NY, USA) directed against tau protein phosphorylated at serine-202 (pS202), or monoclonal antibody Tau 5 (Dr. Lester Binder, Northwestern University Medical School, Chicago, IL, USA) directed at phosphorylation-independent tau protein (total tau). In order to compare the Tau 5 immunolabeling patterns between the experimental and control samples, triplicate densitometry measurements were conducted on each of the 3 tau isoform bands (maximum for each band) and summed. We used a commercial enzyme-linked immunosorbent assay (ELISA) kit to quantitate murine-specific tau protein phosphorylated at serine 199 (Invitrogen, Carlsbad, CA, USA). Frozen brain samples were homogenized in eight volumes of 5 M guanidine-HCl 50 mM Tris (pH 8) followed by five passes in a glass teflon homogenizer. Homogenates were mixed for 3 hrs, diluted into PBS

containing protease inhibitors, and centrifuged for 20 min at 16,000 g. Supernatants were diluted and assayed in quadruplicate for phosphorylated tau according to the manufacturer's instructions.

Statistical Analyses. Comparisons of axonal conduction velocity and LTP magnitude between sham-blast control mice and blast-exposed mice 14 and 28 days post-exposure were made using repeated-measures multi-factorial ANOVA with Bonferroni-Dunn post-hoc correction. Neurobehavioral assessment was conducted using an open-field test and Barnes maze (Med-Associates, St. Albans, VT). Longitudinal data were compared between blast-exposed mice and sham-blast controls using repeated measures ANOVA. Memory retrieval was evaluated by Student's t-test for two-tailed data. Immunoblot densitometry and biochemical data were evaluated by two-tailed Student's t-test. Levels of significance are indicated as follows: *, $P < 0.05$; **, $P < 0.01$; ***, $P < 0.001$. Statistical significance was pre-set at $P < 0.05$.

References

1. J. P. Vonsattel, H. Aizawa, P. Ge, M. DiFiglia, A. C. McKee, M. MacDonald, J. F. Gusella, G. B. Landwehrmeyer, E. D. Bird, E. P. Richardson, Jr., et al., An improved approach to prepare human brains for research, *J Neuropathol Exp Neurol* **54**, 42-56 (1995).
2. A. C. McKee, R. C. Cantu, C. J. Nowinski, E. T. Hedley-Whyte, B. E. Gavett, A. E. Budson, V. E. Santini, H. S. Lee, C. A. Kubilus, R. A. Stern, Chronic traumatic encephalopathy in athletes: progressive tauopathy after repetitive head injury, *J Neuropathol Exp Neurol* **68**, 709-735 (2009).
3. A. C. McKee, B. E. Gavett, R. A. Stern, C. J. Nowinski, R. C. Cantu, N. W. Kowall, D. P. Perl, E. T. Hedley-Whyte, B. Price, C. Sullivan, P. Morin, H. S. Lee, C. A. Kubilus, D. H. Daneshvar, M. Wulff, A. E. Budson, TDP-43 proteinopathy and motor neuron disease in chronic traumatic encephalopathy, *J Neuropathol Exp Neurol* **69**, 918-929 (2010).
4. I. Cernak, A. C. Merkle, V. E. Koliatsos, J. M. Bilik, Q. T. Luong, T. M. Mahota, L. Xu, N. Slack, D. Windle, F. A. Ahmed, The pathobiology of blast injuries and blast-induced neurotrauma as identified using a new experimental model of injury in mice, *Neurobiol Dis* **41**, 538-551 (2011).
5. V. E. Koliatsos, I. Cernak, L. Xu, Y. Song, A. Savonenko, B. J. Crain, C. G. Eberhart, C. E. Frangakis, T. Melnikova, H. Kim, D. Lee, A mouse model of blast injury to brain: initial pathological, neuropathological, and behavioral characterization, *J Neuropathol Exp Neurol* **70**, 399-416 (2011).
6. J. Lu, K. C. Ng, G. S. Ling, J. Wu, J. F. Poon, E. M. Kan, M. H. Tan, Y. J. Wu, P. Li, S. Moochhala, E. Yap, L. K. Lee, A. L. Teo, I. B. Yeh, D. M. Sergio, F. Chua, S. D. Kumar, E. A. Ling, Effect of Blast Exposure on the Brain Structure and Cognition in the Macaca Fascicularis, *J Neurotrauma*, [Epub ahead of print; 2011]. PMID: 21639720
7. C. A. Barnes, Memory deficits associated with senescence: a neurophysiological and behavioral study in the rat, *J Comp Physiol Psychol* **93**, 74-104 (1979).
8. S. Saman, W. Kim, M. Raya, Y. Visnick, S. Miro, B. Jackson, A. C. McKee, V. E. Alvarez, N. C. Lee, G. F. Hall, Exosome-associated tau is secreted in tauopathy models and is selectively phosphorylated in cerebrospinal fluid (CSF) in early Alzheimer's Disease, *J. Biol. Chem*. **287**, 3842-3849 (2012).

Table S1. Summary of antibodies used in this study.

Protein Target	Antibody	Epitope	Type	Assay*	Source
APP	22C11	aa66-81	Mouse mAb	IHC	Millipore
Pan-Tau	Tau-46	Tau protein	Mouse mAb	IHC	Dr. G. Hall
Pan-Tau	Tau-5	Tau protein	Mouse mAb	WB	Dr. L. Binder
Phospho-Tau	CP-13	pS202/pT205	Mouse mAb	IHC, WB	Dr. P. Davies
Phospho-Tau	PHF-1	pS396/404	Mouse mAb	IHC	Dr. P. Davies
Phospho-Tau	AT270	pT181	Mouse mAb	WB	Innogenetics
Phospho-Tau	AT8	pS202/pT205	Mouse mAb	IHC	Pierce Endogen
Phospho-Neurofilament	SMI-34	pNFH/M	Mouse mAb	IHC	Abcam
Phospho-Neurofilament	SMI-31	pNFH/M	Mouse mAb	IHC	Covance
HLA-DR II (MHC)	LN-3	HLA-DR	Mouse mAb	IHC	Invitrogen
Glial Fibrillary Acidic Protein	GA5	GFAP	Mouse mAb	IHC	Millipore
Choline Acetyltransferase	68779	ChaT	Sheep pAb	IHC	Abcam

*IHC, immunohistochemistry; WB, western blot (protein immunoblot)

Table S2. Murine blast neurotrauma model blast parameters.

Shock Tube Blast Parameters	Mean	SD	% RSD
Rupture Pressure (kPag)	303	9	3
Incident Static Pressure (kPag)	77	2	3
Pressure Rise Time (µs)	38	3	7
Compressive Phase Duration (ms)	4.8	0.1	1.0
Compressive Phase Impulse (kPag•ms)	167	4	2
Reflected Pressure (kPag)	127	3	2
Pressure Rise Time (µs)	23	0.2	1
Compressive Phase Duration (ms)	4.1	0.1	2
Compressive Phase Impulse (kPag•ms)	258	7	3
Shock wave Velocity (Mach)	1.26	0.04	2
Blast Wind Velocity (m/s)	150*		
Blast Wind Velocity (mph)	336*		

*Calculated value based on empirically-determined pressure measurements.

Table S3. Shock tube blast compared to equivalent explosive blast.

Blast Parameter	Shock Tube[1]	ConWep[2]
Blast System	Compressed Gas Shock Tube	ConWep Algorithm
Blast Wave Initiation	Burst Pressure 303 kPag	C4 Explosive 4.5 kg
TNT Equivalence (kg)	5.8[2]	5.8[2]
Distance from Source (m)	4.1	5.5
Static Incident Pressure (kPag)	77	77
Positive Phase Duration (ms)	4.8	4.9
Incident Impulse (kPag•ms)	167	112
Shockwave Velocity (Mach)	1.3	1.3
Peak Particle Velocity (m/s)	150	143
Peak Blast Wind Velocity (mph)	336	321

[1] Blast is comparable to a commonly encountered improvised explosive device (IED) constructed of a 120 mm mortar round with blast equivalence of 4.53 kg of TNT (http://www.gwu.edu/~nsarchiv/IMG/soldiershandbookiraq.pdf).

[2] Blast equivalency: 4.50 kg Compostion C-4 (5.76 kg TNT) at 5.53 meters calculated using ConWep analysis conducted by William C. Moss, Ph.D., Lawrence Livermore National Laboratory, Livermore, CA. ConWep software is based on Kingery C. and Bulmash G. (1984) *Airblast Parameters from TNT Spherical Air Burst and Hemispherical Surface Burst.* Technical Report ARBRL-TR-02555, U.S. Army Ballistic Research Laboratory Proving Ground, Aberdeen, MD. U.S. Army Technical Manual TM 5-855-1, Fundamentals of Protective Design for Conventional Weapons, 1986 (http://www.military-info.com/MPHOTO/p021c.htm). See also Hyde D.W., CONWEP 2.1.0.8, Conventional Weapons Effects Program, United States Army Corps of Engineers, Vicksburg, MS, 2004.

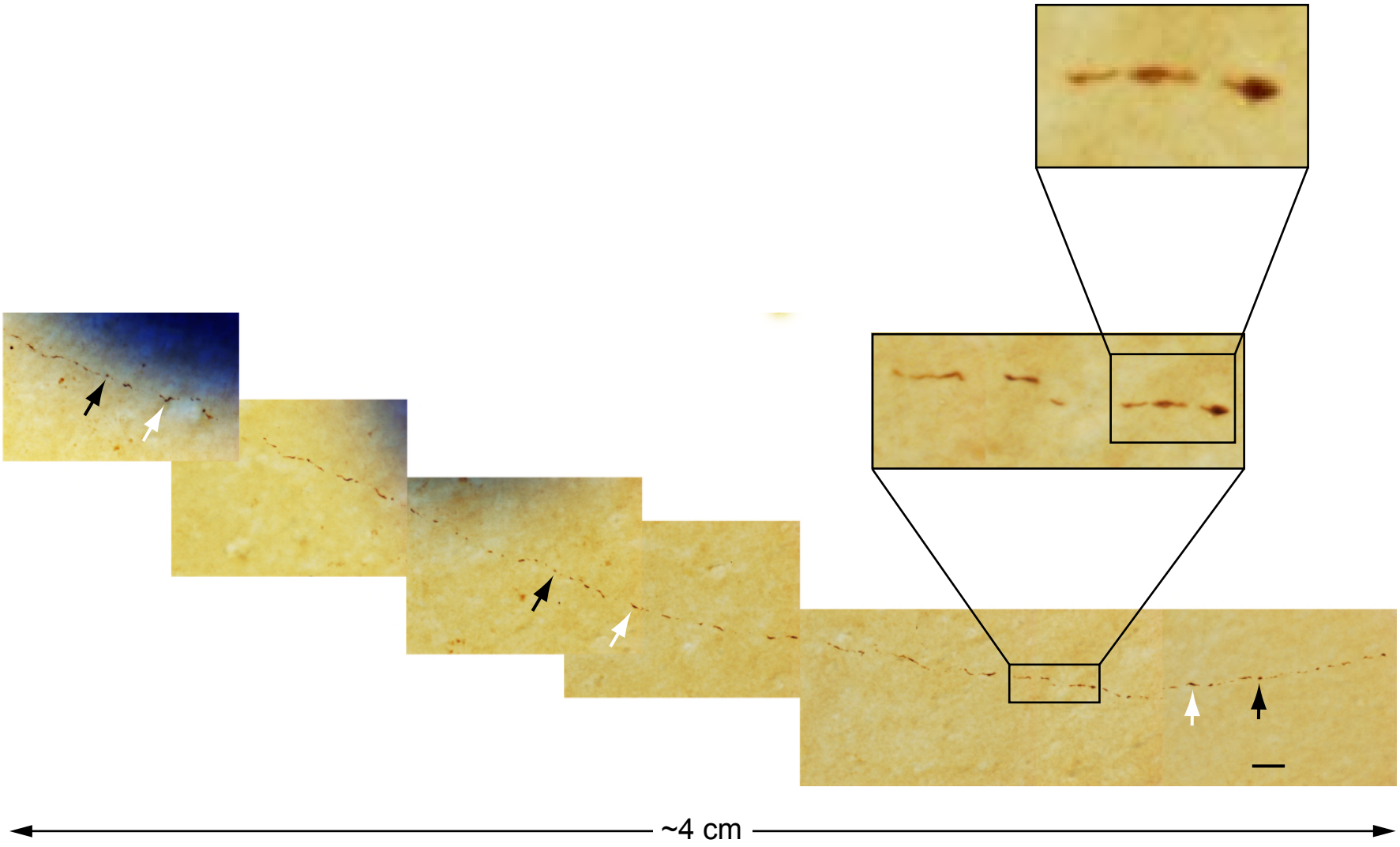

Fig. S1. Phosphorylated tau axonopathy in a single axon from the brain of a 22-year-old male military veteran with exposure to a single improvised explosive device blast and persistent blast-related traumatic brain injury symptoms.
Micrographic montage demonstrating a CP13-immunoreactive axon with beaded (black arrows) and lentiform (white arrows) varicosities along a ~4 cm length in the external capsule. Calibration bar, 50 μm. Clinical details can be found in *Results* (Case 3).

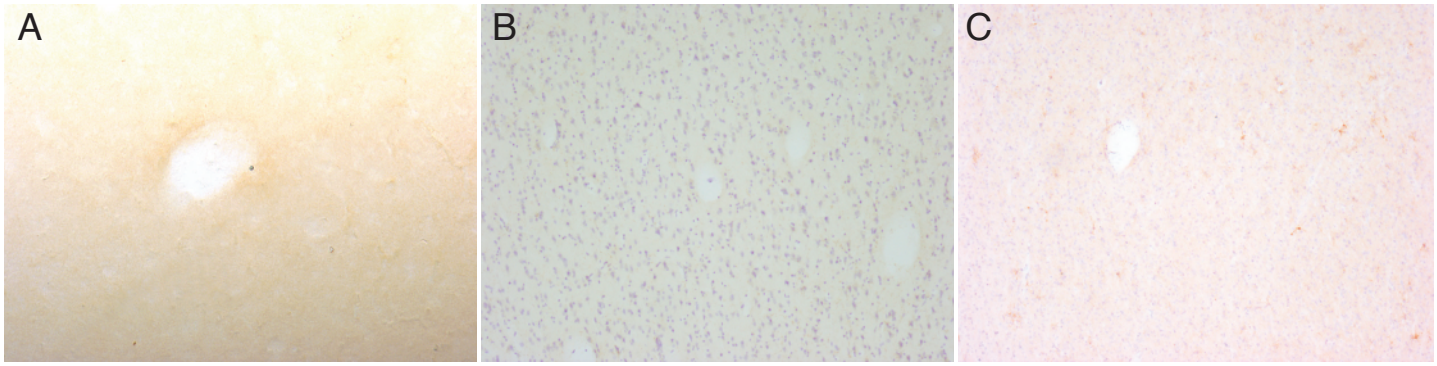

Fig. S2. Absence of CTE neuropathology in a representative postmortem human brain from 21-year-old male control subject without known history of blast exposure or concussive injury. (**A**) Absence of specific CP-13 immunostaining for phosphorylated tau protein (pS202/pT205) in the dorsolateral prefrontal cortex. Magnification, X20. (**B**) Absence of specific AT8 immunostaining for phosphorylated tau protein (pS202/pT205) in the dorsolateral prefrontal cortex. Magnification, X10. (**C**) Absence of specific LN3 immunostaining for MHC class II-positive microglia in the subcortical frontal white matter. Magnification, X10. Sections were counterstained with cresyl violet.

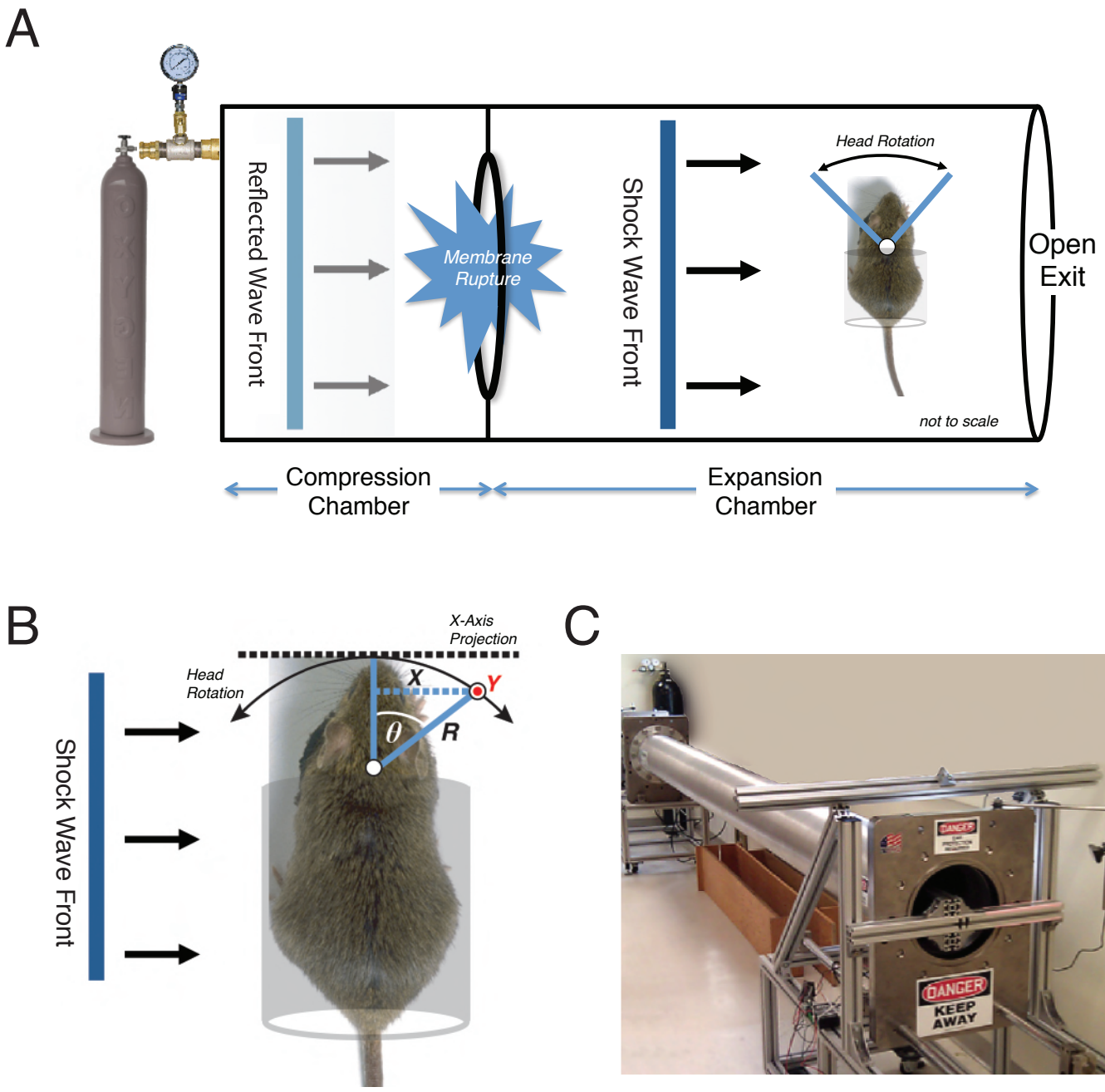

Fig. S3. Schematic and geometry of the murine blast neurotrauma shock tube system. (**A**) Schematic of the purpose-designed shock tube blast neurotrauma system used in this study. Pressurized gas is delivered into the closed system of the pre-burst compression chamber. Abrupt rupture of a mylar membrane diaphragm separating the compression and expansion chambers initiates a blast shock wave front that traverses the long axis of the 4.5 m shock tube at supersonic velocity (Mach 1.26 ± 0.04; see Supplemental Table S2). (**B**) Geometry of blast-induced head motion. Anesthetized mice were secured in a thoracic-protective restraint system positioned inside the shock tube exactly 0.56 m from the open exit of the expansion chamber. High-speed videography enabled precise tracking of a single point on the head in the indicated projected planes of motion. The projected path and kinematics of the head during blast exposure was determined from frame-capture images at a capture rate of 100,000 fps. To translate from the recorded projected head rotation path (X,Y), a motion radius (R) was determined using a pivot point between the scapulae and an endpoint at the snout. The rotational angle of the head (θ) was calculated trigonometrically. (**C**) Murine blast neurotrauma system was developed in collaboration with the Fraunhofer Center for Manufacturing Innovation at Boston University, Brookline, MA, and operated at the Neurotrauma Laboratory, Boston University School of Medicine, Boston, MA.

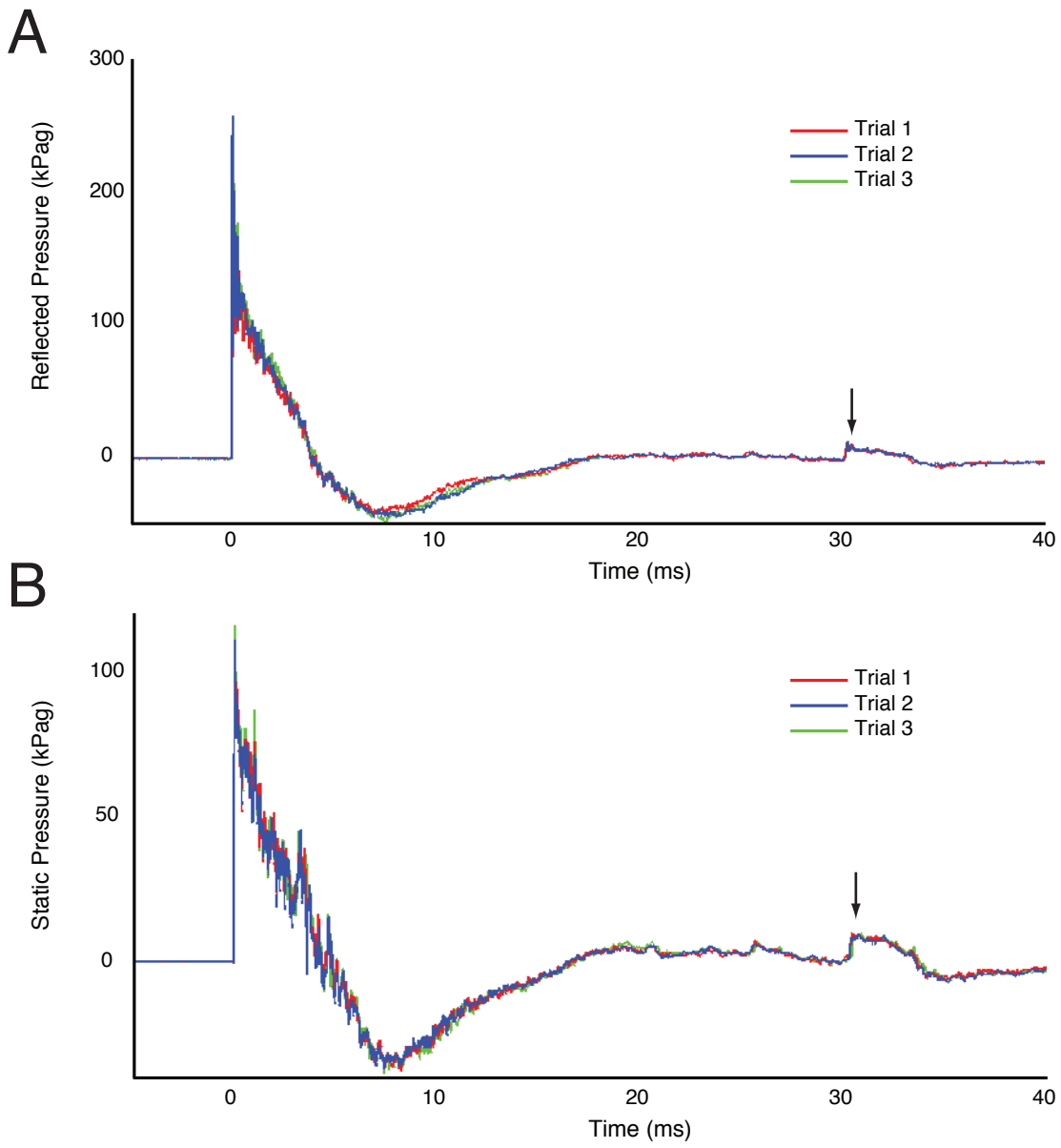

Fig. S4. Reproducibility of shock tube blast static and reflected pressure.
(**A**) Reproducibility of shock tube blast wave pressure waveforms assessed with pressure transducer positioned in the reflected (face-on) orientation relative to the direction of the oncoming shock wave. (**B**) Same shock tube blast waves assessed with pressure transducer positioned in the incident static (side-on) orientation. Note that the static component does not capture dynamic pressure associated with particle motion. The signal at 30 ms (arrow) detected in both orientations was identified as a small reflected wave originating outside the shock tube. Peak pressure was determined by linearly extrapolating the decay of the curve to shock arrival time. Note that the initial pressure spike represents an artifact associated with diffraction at the pressure transducer. In the case shown, the peak static overpressure was 80 kPag with a diffraction artifact spike ~120 kPag. Pressure data was processed with 20 kHz low-pass filtering.

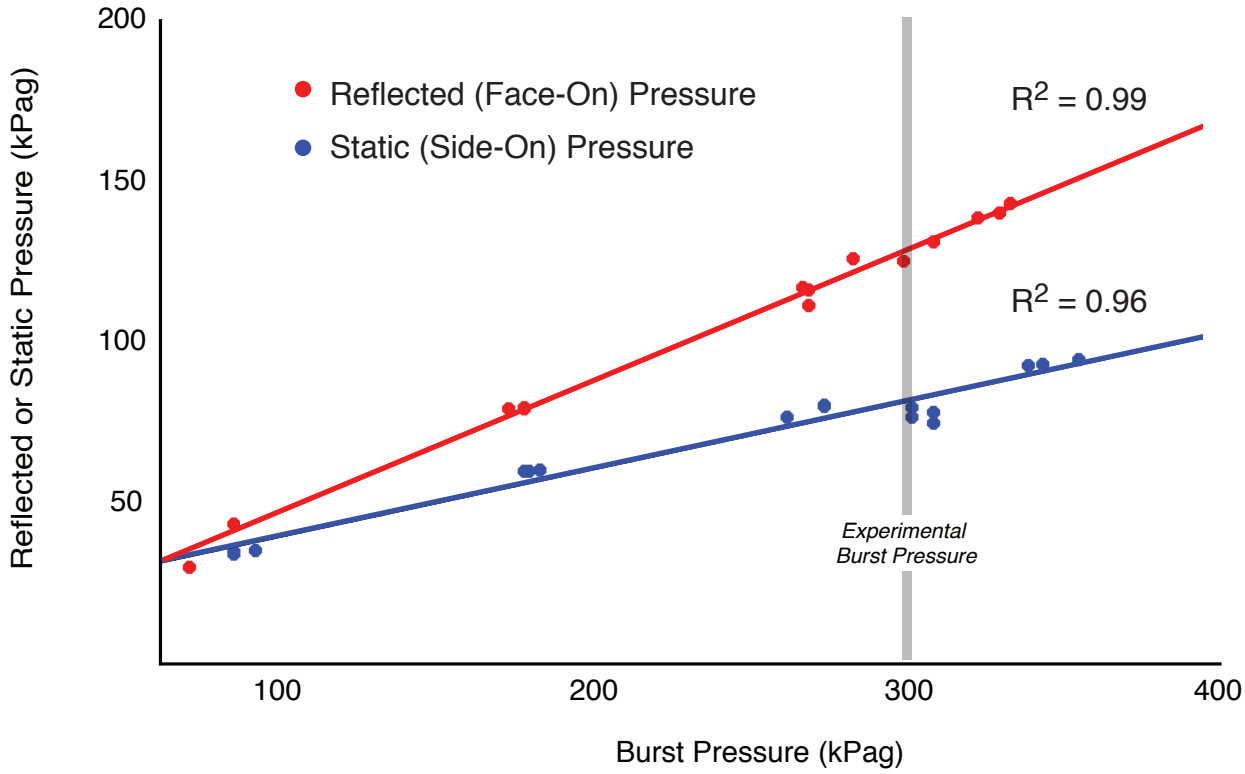

Fig. S5. Peak reflected and static incident pressure as a function of shock tube burst pressure. Reflected (face-on) and static incident (side-on) pressure demonstrate linear proportionality (.i.e., peak pressure as a function of rupture pressure) over ranges relevant to human blast neurotrauma.

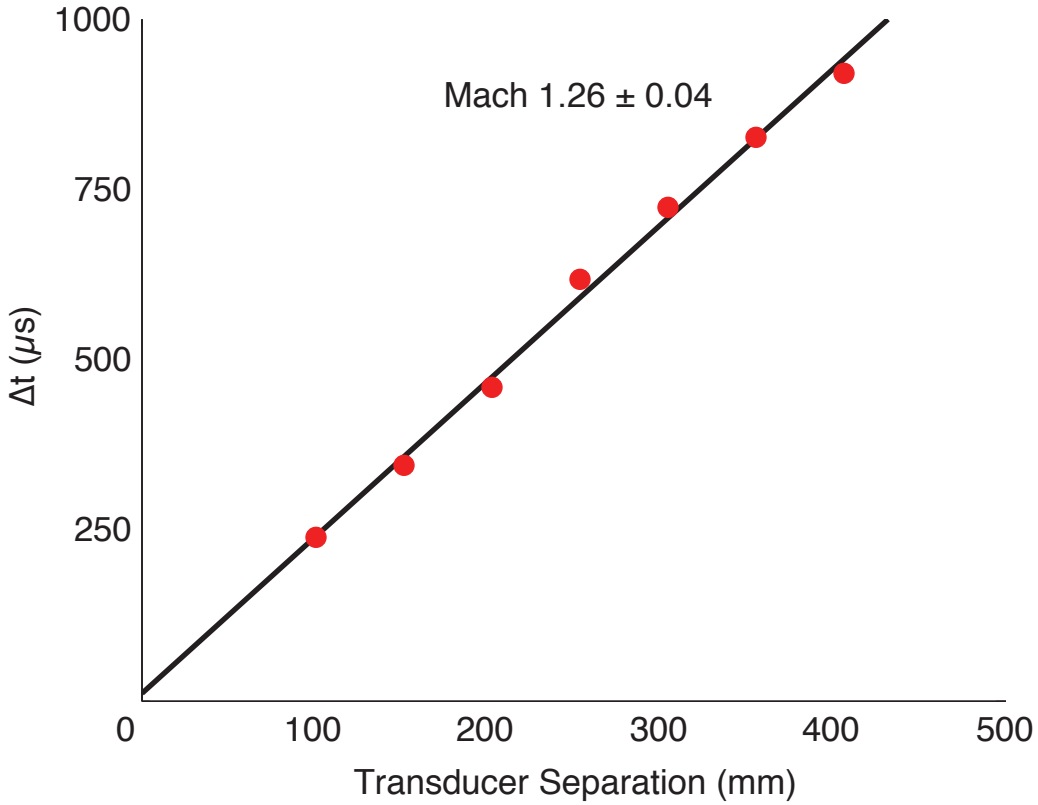

Fig. S6. Shock wave velocity (Mach) regression analysis.
Arrival time of the shock wave as a function of the position of the static (side-on) free-field pressure transducer in the shock tube. The pressure transducer was flush mounted inside the shock tube. The slope of the linear regression was 2.32 μs/mm (R^2 = 1.00). The corresponding shock wave velocity yielded a calculated Mach number of 1.26.

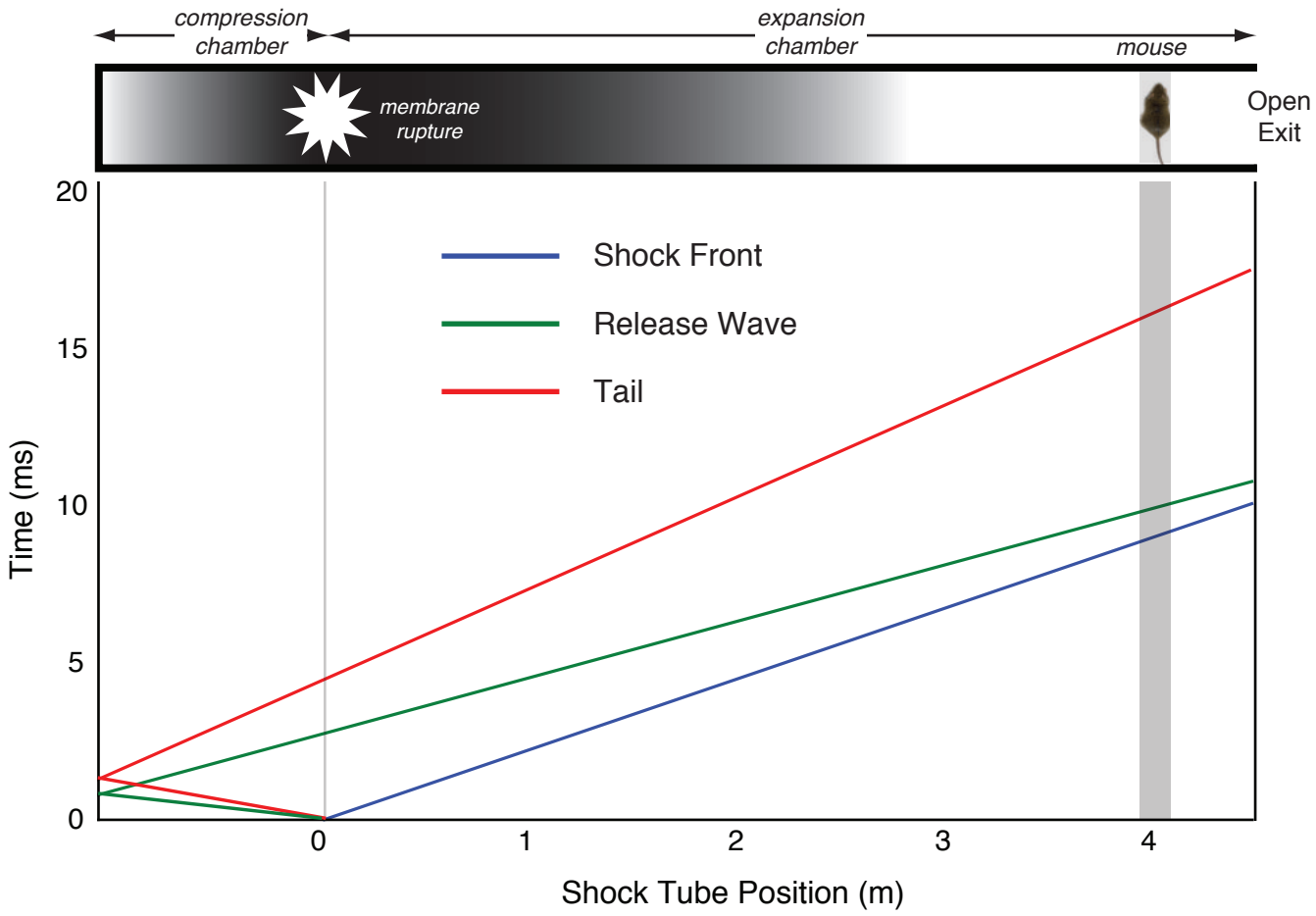

Fig. S7. X-T wave diagram demonstrating positional and temporal features of the blast shock wave. Blast shock wave front (blue line), shock wave tail (red line), and release wave corresponding to the trailing edge of the compression phase (green line) were calculated according to gas dynamic equations (Liepman & Roshko, *Elements of Gas Dynamics,* Wiley & Sons, New York, 1957). Interactions between counter-propagating waves in the compression section have been ignored. Wave transmission is shown from the blast origin (x = 0) at the interface between the compression and expansion chambers of the shock tube. Mice were positioned 0.56 m from the open exit of the shock tube. Note that near the exit of the shock tube, the release wave has almost caught up with the shock wavefront in agreement with measured waveform at a distance of 4.06 m. The predicted waveform is based on theoretical considerations and the timing of the shock wave at 4.06 m. These data are in good agreement with the amplitude, duration, impulse, and shape of the blast waveform measured experimentally (Fig. 2).

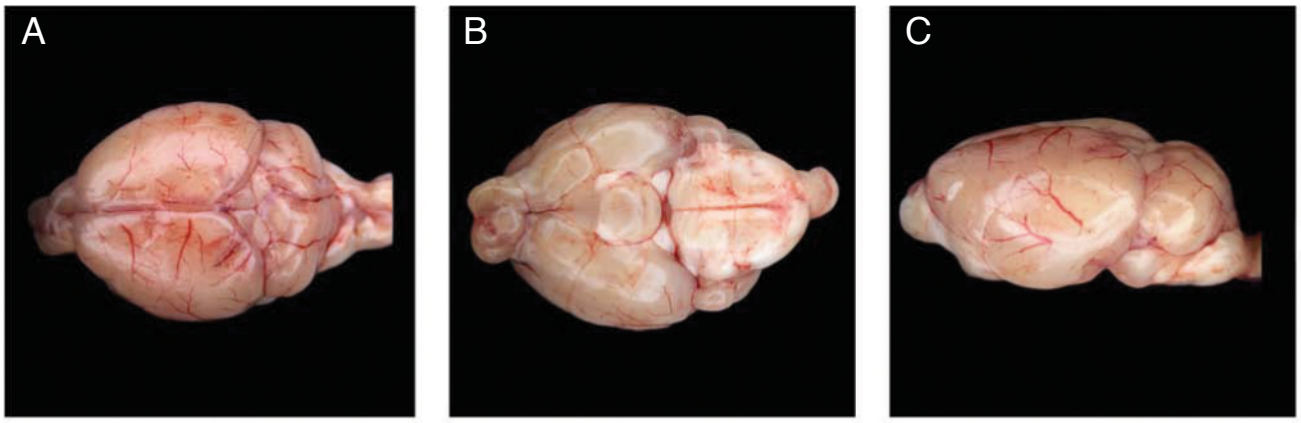

Fig. S8. Unperfused C57BL/6 mouse brain 2 weeks after single shock tube blast exposure. Representative unperfused brain from adult male wildtype C57BL/6 mice sacrificed two weeks after exposure to a single shock tube blast did not exhibit gross brain pathology, contusion, necrosis, hematoma, petechial hemorrhage, or focal tissue damage. Dorsal (**A**), ventral (**B**), and lateral (**C**) surfaces of a representative freshly dissected unperfused brain.

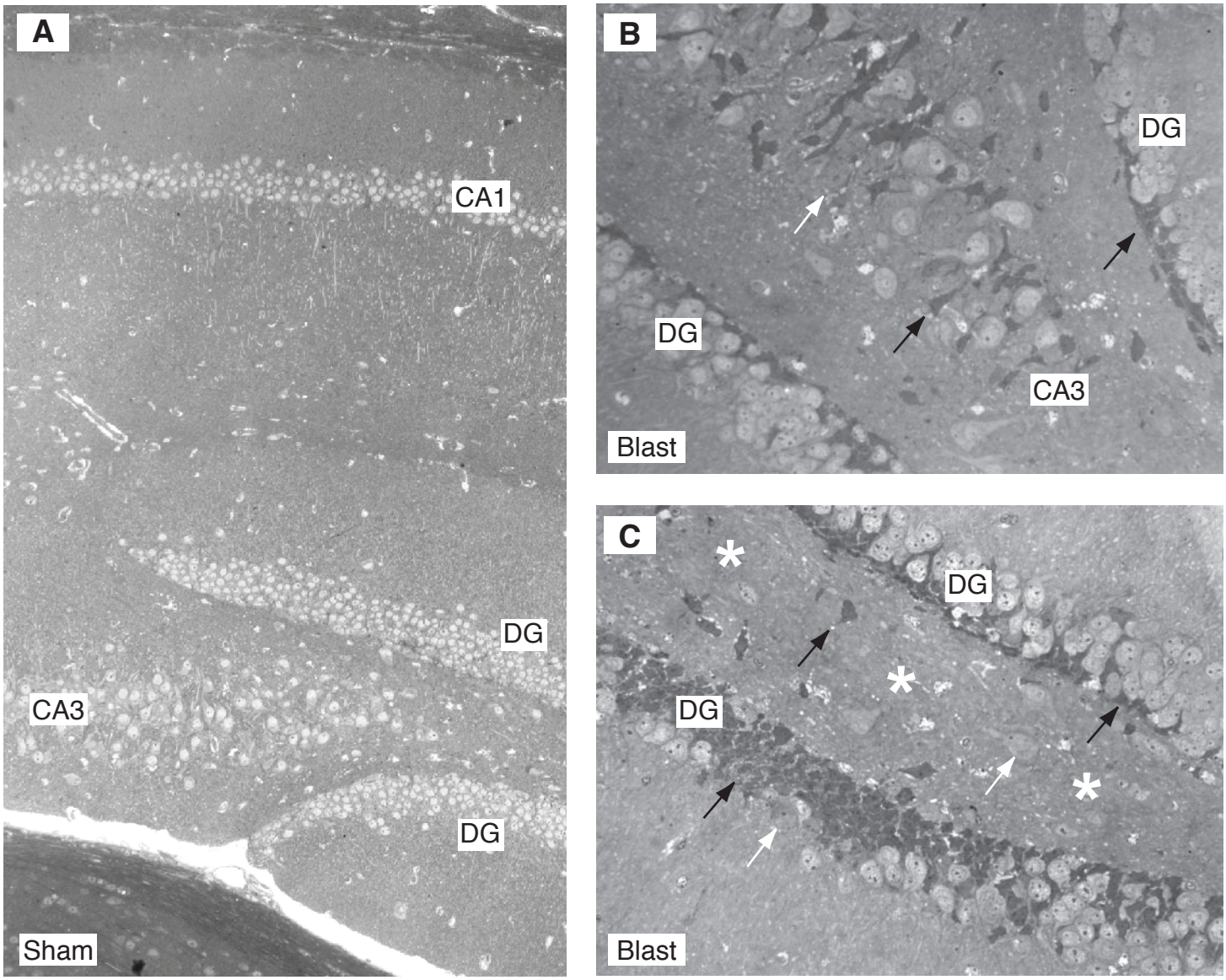

Fig. S9. Neuropathology in the CA3 field and dentate gyrus in a C57BL/6 mouse brain two weeks after exposure to a single shock tube blast.

(**A**) Semi-thick sections of the hippocampus in a C57BL/6 mouse brain two weeks after control exposure to sham blast. Normal histological structure in the hippocampal CA1 and CA3 fields and dentate gyrus. (**B,C**) Toluidine blue-stained semi-thick section of the hippocampus and dentate gyrus in a C57BL/6 mouse brain two weeks after exposure to a single shock tube blast. In addition to neuropathology in the CA1 field (Fig. 4), the CA3 field and dentate gyrus also demonstrate evidence of extensive neuronal damage, including local neuronal pyknosis (black arrows, **B,C**), chromatolysis (white arrows, **B,C**) and dropout (asterisk, **C**).

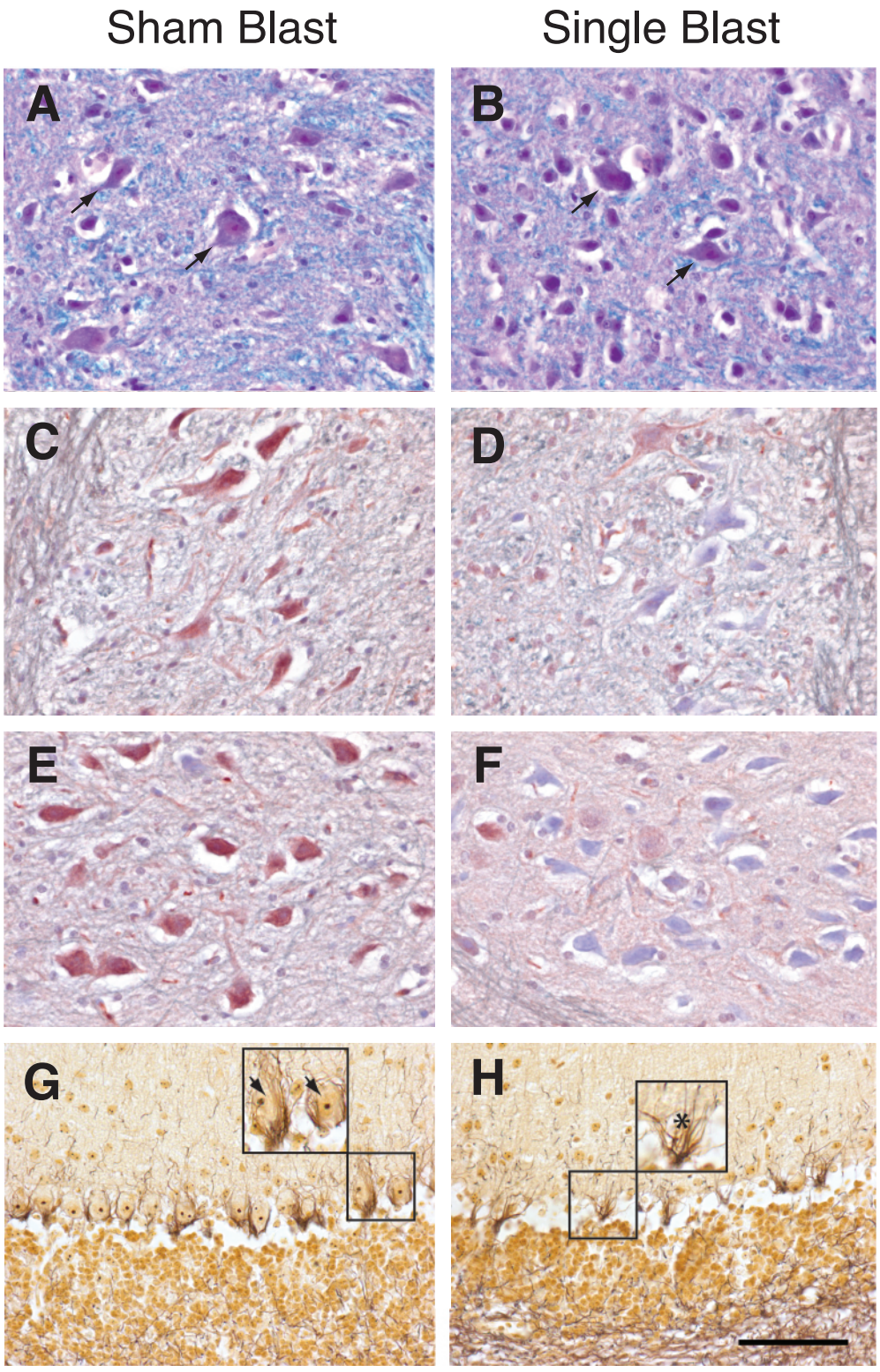

Fig. S10. Decreased choline acetyltransferase (ChAT) immunoreactivity in the brainstem and neuronal dropout in the cerebellum of C57BL/6 mice two weeks after exposure to a single shock tube blast. (**A**, **B**) Luxol fast blue/hematoxylin and eosin staining shows cervical spinal cords well-populated with intact motor neurons (arrows) in mice exposed to sham blast (A) or single blast (B). (**C**,**E**) Immunohistochemical staining for ChAT in sham blast mice shows robust staining of motor neurons of the cervical spinal cord (C) as well as motor neurons in the nucleus of cranial nerve XII (E). (**D**,**F**) In contrast, ChAT immunostaining is markedly decreased in cervical spinal cord (D) and CN XII motor neurons (F) two weeks after single blast exposure. (**G**) Bielschowsky silver stain reveals intact cerebellar Purkinje cells (arrows, inset) associated with basket cell axons in sham blast mice. (**H**) Focal loss of cerebellar Purkinje cells and presence of empty baskets (asterisk, inset) in blast-exposed mice. Bar, 100 μm.

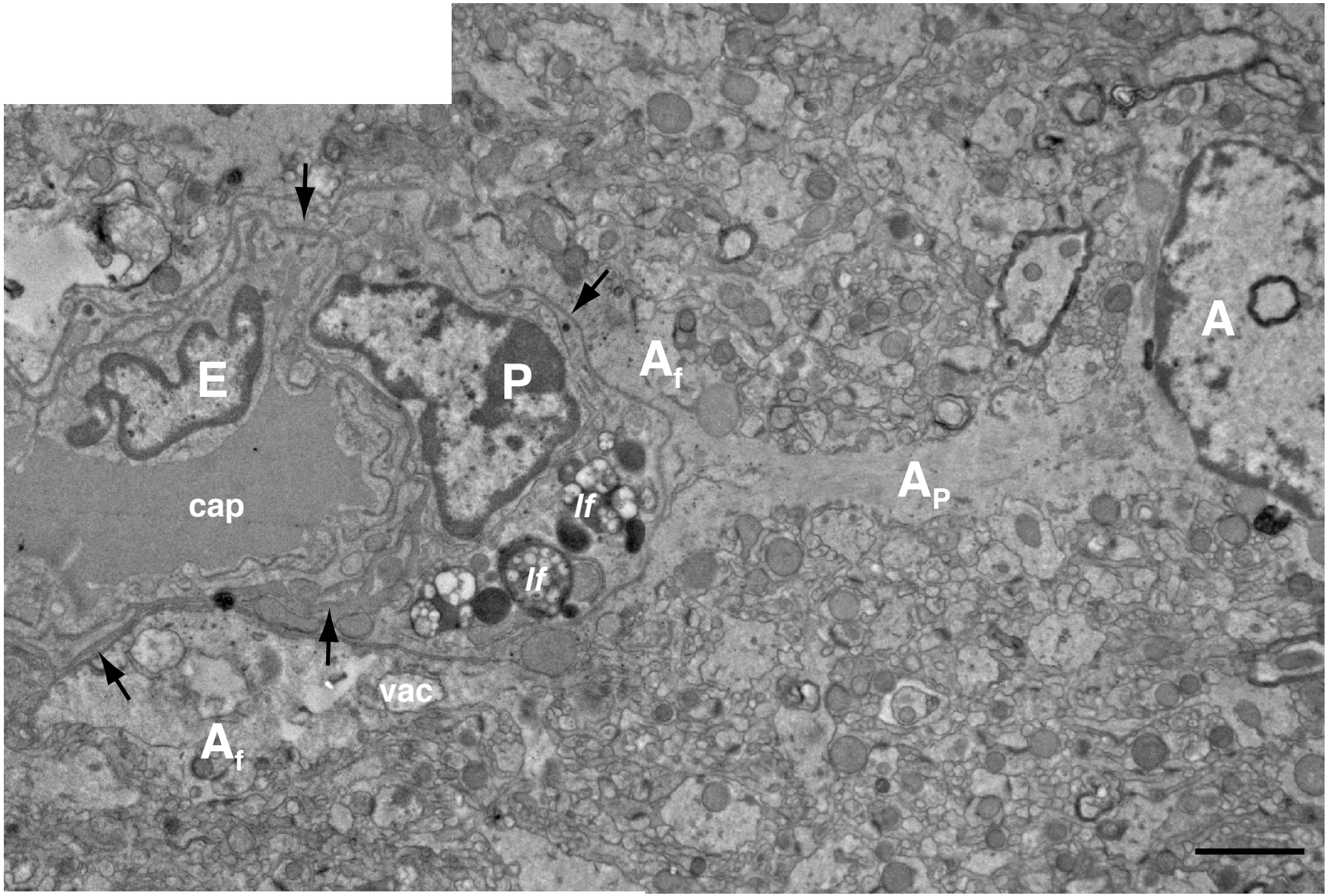

Fig. S11. Electron micrographic montage of the hippocampus CA1 field in a C57BL/6 mouse brain two weeks after exposure to a single shock tube blast.

EM montage of the CA1 field *stratum radiatum* shows an enlarged field of the same perivascular profile presented in Fig. 4L. A pale, hydropic astrocyte (A), astrocytic process (Ap), and pathologically swollen astrocytic end-feet (Af) in the vicinity of an irregularly shaped capillary (cap) with a thickened, tortuous basal lamina (black arrows). An endothelial cell (E) with an abnormally contoured multilobed nucleus is located near a perivascular pericyte (P). A process containing lipofuscin granules (lf) is also evident. Bar, 2 μm.

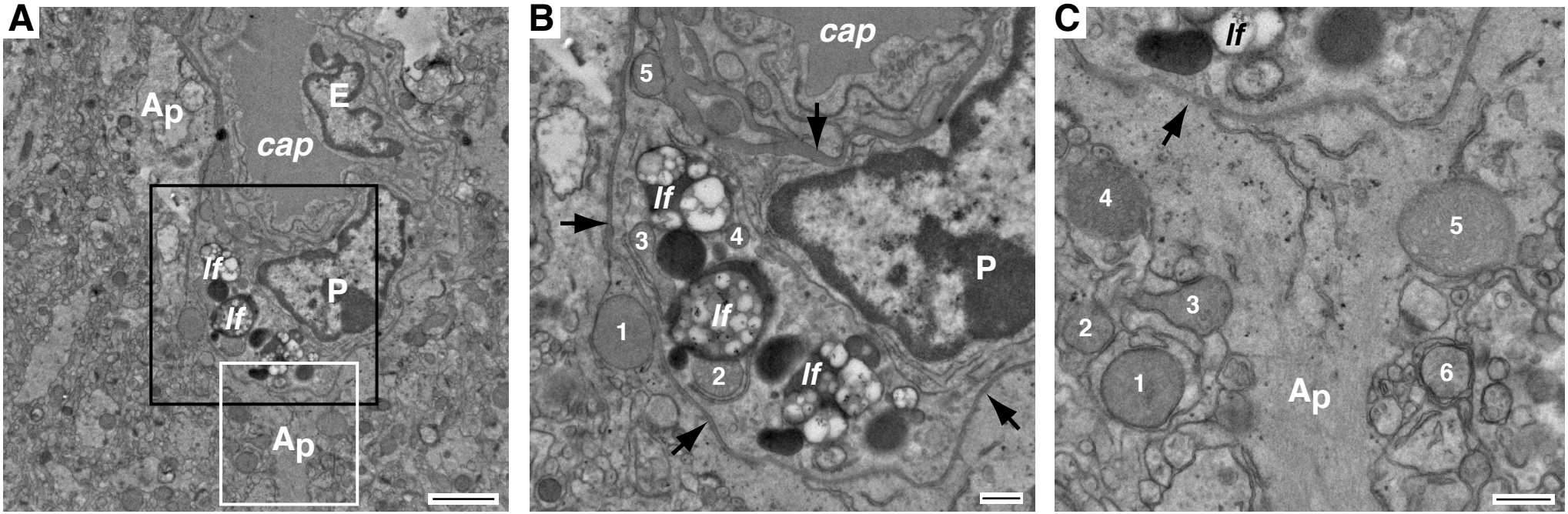

Fig. S12. High-magnification EM micrographs of the hippocampus CA1 field in a C57BL/6 mouse brain two weeks after single blast exposure. These EM micrographs show selected enlarged fields of the same hydropic perivascular profile presented in Fig. 4L and fig. S10. (**A**) Hydropic perivascular region of the CA1 field demonstrating an edematous astrocytic process (Ap) surrounding an irregularly shaped capillary (cap). An abnormal endothelial cell (E) with a multilobed nucleus is located near a pericyte (P). Lipofuscin granules (lf) are also evident. Black box corresponds to high-magnification micrograph in (B). White box corresponds to high-magnification micrograph in (C). Bar, 2 μm. (**B**) High-magnification EM micrograph showing lipofuscin granules (lf) and degenerating mitochondria (numbered 1 to 5). A capillary (cap) with a grossly thickened, tortuous basal lamina (black arrows) and adjacent pericyte (P) are also evident. Bar, 500 nm. (**C**) High-magnification EM micrograph showing a perivascular astrocytic process (Ap), abnormal mitochondria (numbers 1-6), and lipofuscin granules (lf). A grossly thickened basal lamina (black arrow) is also evident. Bar, 500 nm.

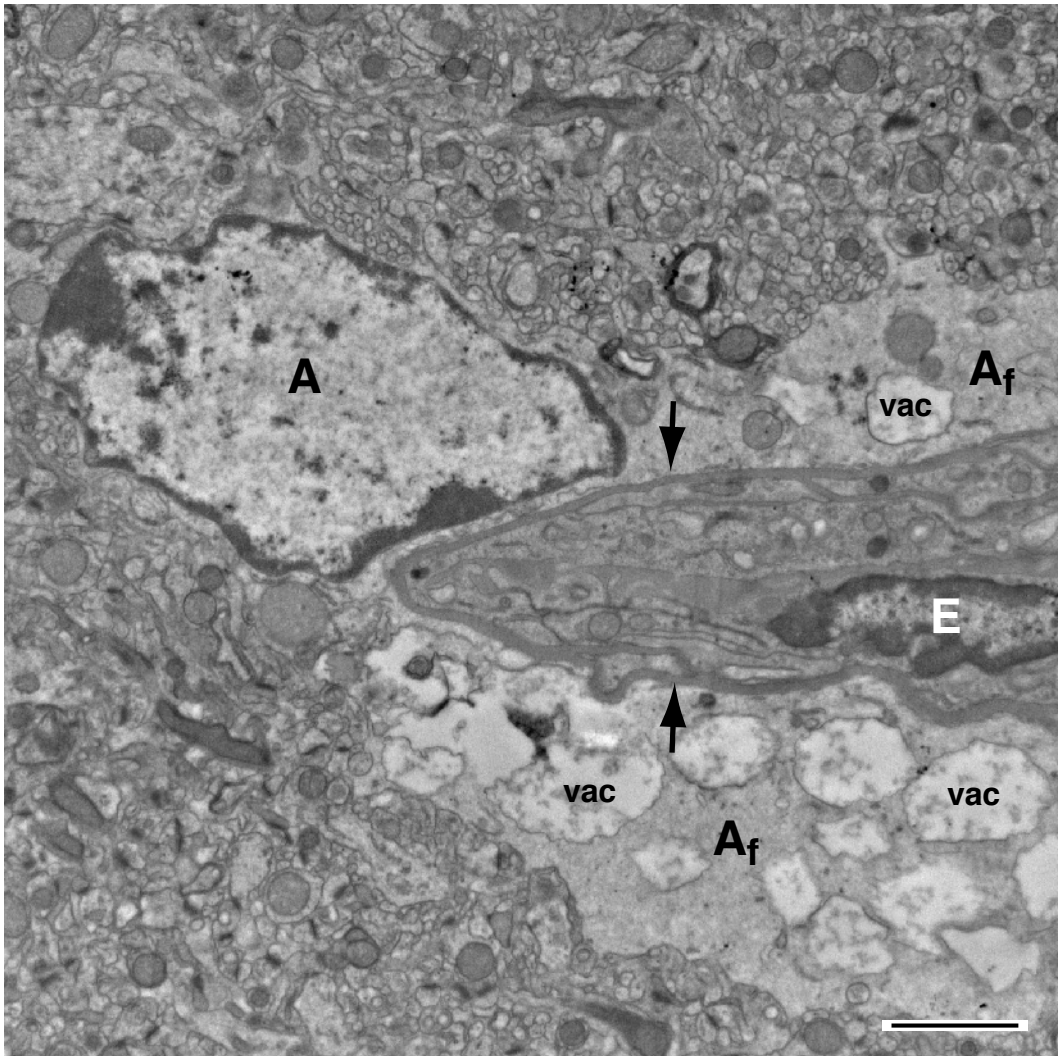

Fig. S13. Perivascular ultrastructural pathology in the hippocampus CA1 stratum radiatum in a C57BL/6 mouse brain two weeks after exposure to a single shock tube blast.
Perivascular astrocyte (A) with edematous end-feet (Af) containing numerous dilated vacuoles (vac). Note the endothelial cell (E) with an irregularly contoured nucleus and grossly thickened basal lamina (black arrows). The capillary lumen is not patent (”string vessel”). Bar, 2 μm.

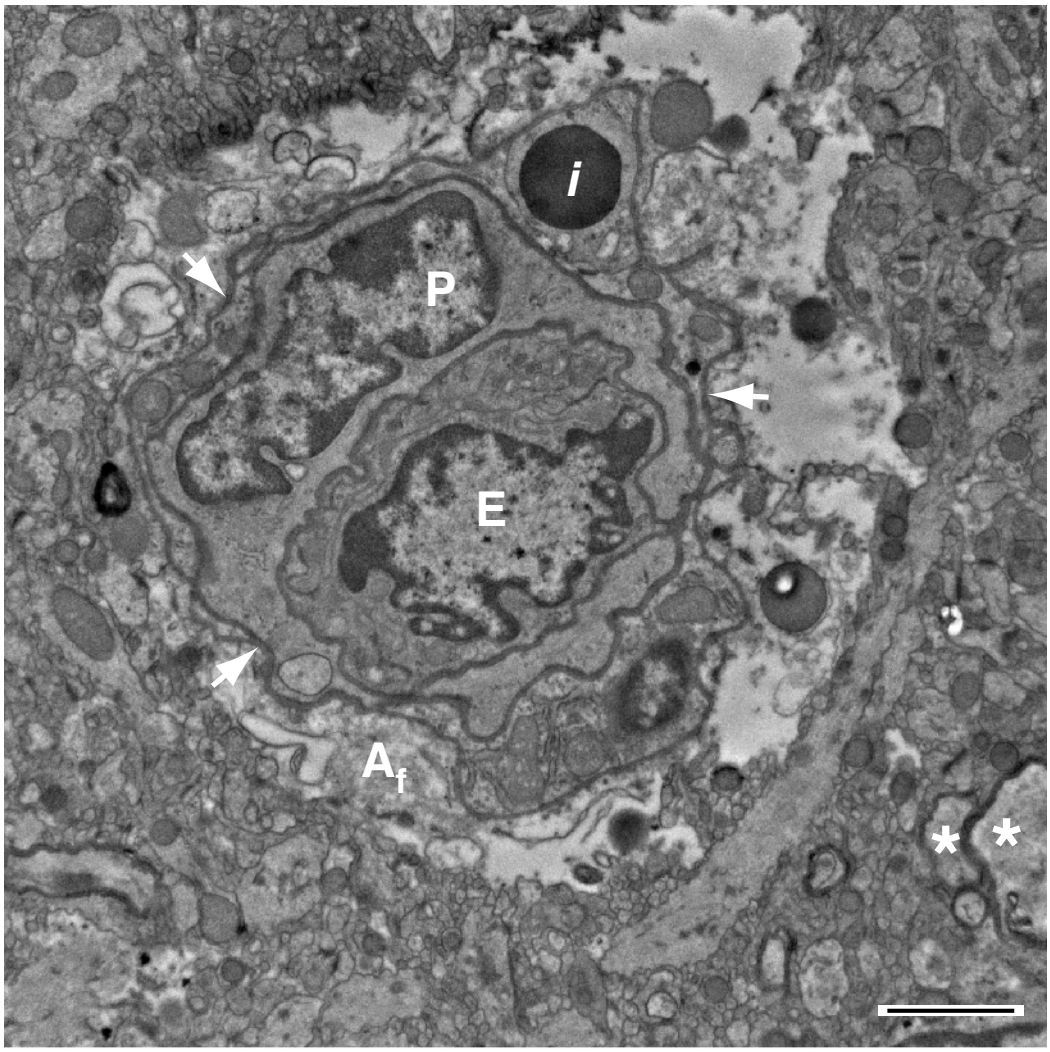

Fig. S14. Perivascular ultrastructural pathology in the hippocampus CA1 stratum radiatum in a C57BL/6 mouse brain two weeks after exposure to a single shock tube blast.
A swollen astrocytic end-foot (Af) surrounds an endothelial cell (E) with an irregularly contoured nucleus and adjacent pericyte (P). A thickened basal lamina (arrows) and electron-dense inclusion granule (i) are also evident. Dysmorphic myelinated axons (asterisks) are present in the surrounding neuropil (asterisks). Bar, 2 μm.

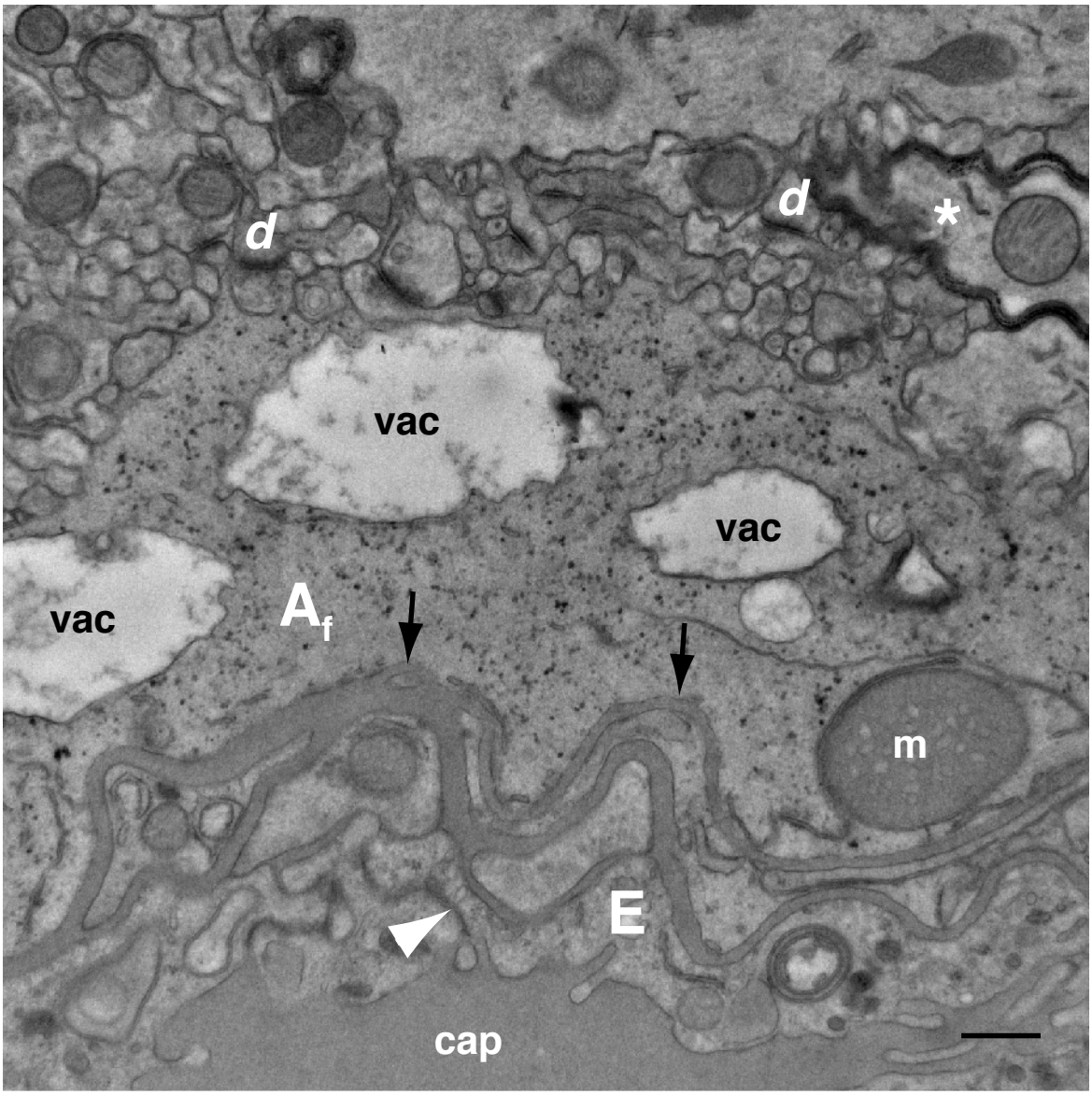

Fig. S15. Perivascular ultrastructural pathology in the hippocampus CA1 stratum radiatum in a C57BL/6 mouse brain two weeks after exposure to a single shock tube blast.
Hydropic astrocytic end-foot (Af) containing numerous vacuoles (vac) and a swollen mitochondrion (m) is associated with a thickened, tortuous basal lamina (black arrows) of an adjacent capillary (cap). Two dendritic spines (d), a dystrophic myelinated axon (white asterisk), and a tight junction (white arrowhead) are also evident in this micrograph. Bar, 500 nm.

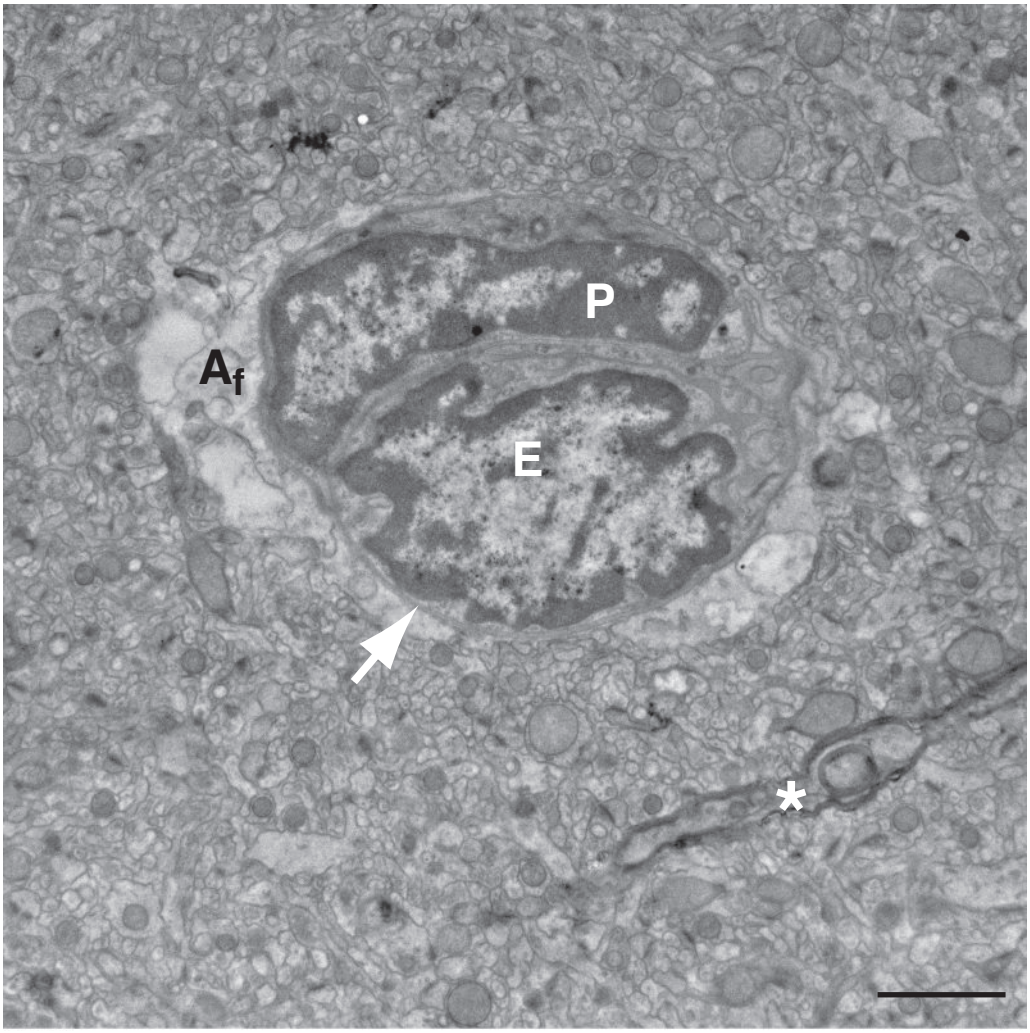

Fig. S16. Perivascular ultrastructural pathology in the hippocampus CA1 stratum radiatum in a C57BL/6 mouse brain two weeks after exposure to a single shock tube blast.
Hydropic astrocytic end-feet (Af) surrounding a pericyte (P), endothelial cell (E), and thickened capillary basal lamina (white arrow). Note that the capillary lumen is not patent, an ultrastructural feature that corresponds to string vessels observable by conventional light microscopy. A dystrophic myelinated axon (asterisk) is also evident. Bar, 2 μm.

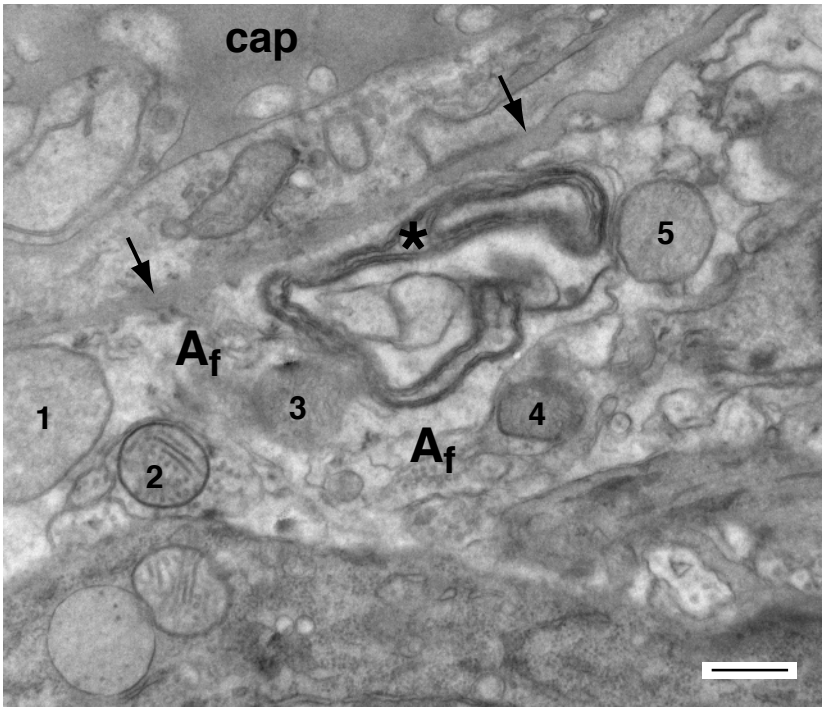

Fig. S17. Myelin figure in the hippocampus CA1 stratum pyramidale in a C57BL/6 mouse brain two weeks after exposure to a single shock tube blast. An edematous astrocytic end-foot (Af) with swollen mitochondria (1-5) and a myelin figure (asterisk). Note the abnormally thickened basal lamina (black arrows) of the adjacent capillary (cap). Bar, 500 nm.

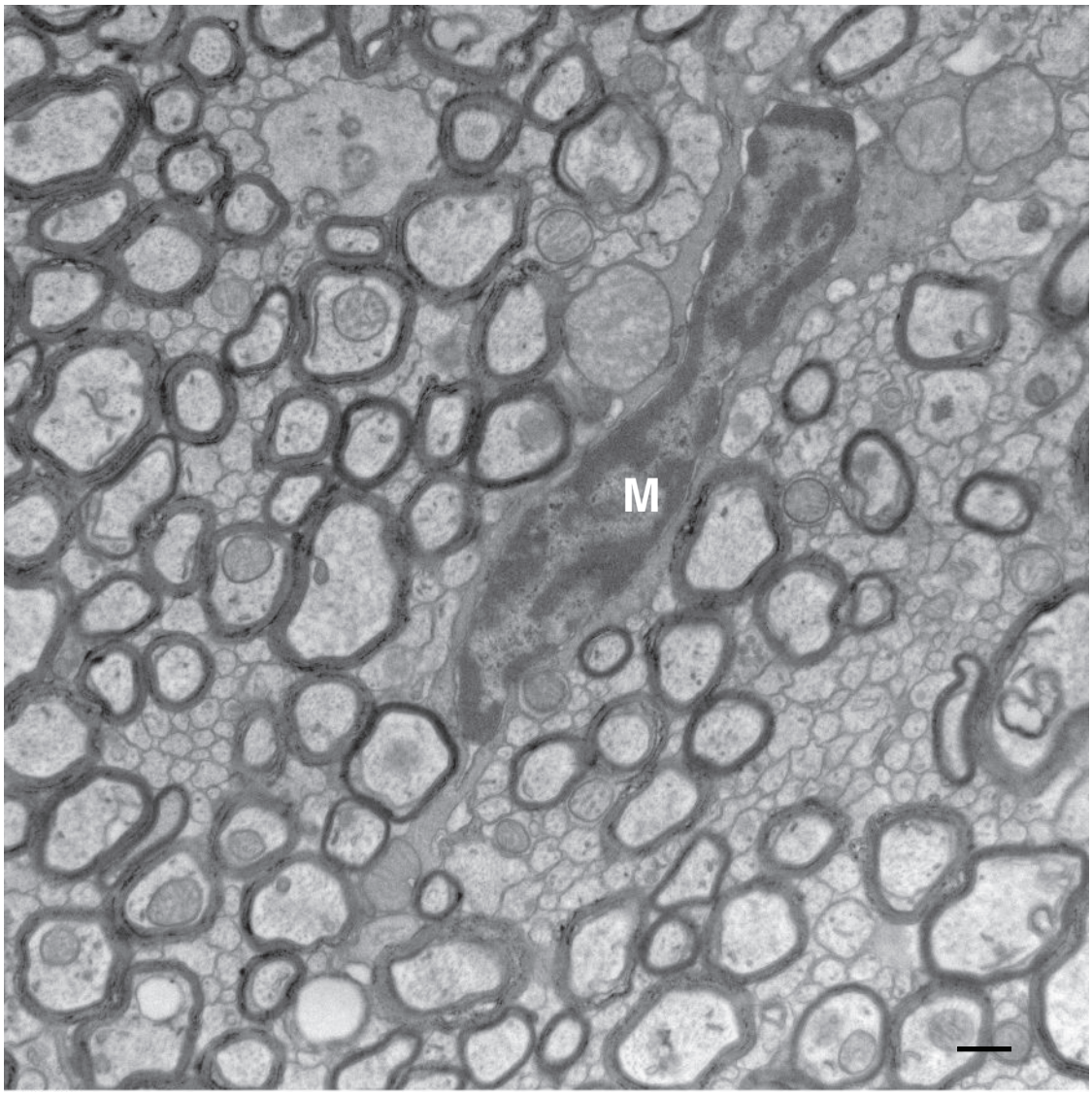

Fig. S18. A microglial cell amidst myelinated axons in the hippocampus CA1 stratum alveus in a C57BL/6 mouse brain two weeks after exposure to a single shock tube blast.
A microglial cell (M) is present a field of myelinated nerve fibers in the hippocampus of a blast-exposed mouse. Note the electron dense nucleus and dark cytoplasm that are characteristic features of microglial cells. Bar, 500 nm.

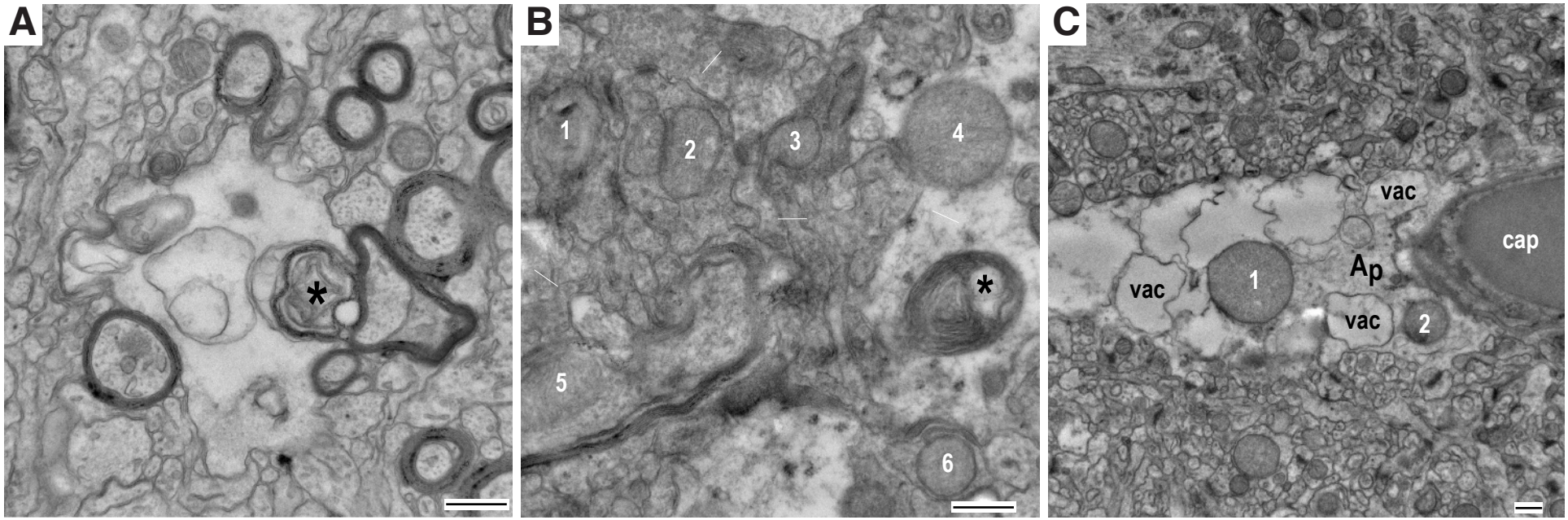

Fig. S19. Autophagy and mitophagy in the hippocampus CA1 field in a C57BL/6 mouse brain two weeks after exposure to a single shock tube blast.

(**A**) Presumptive degenerating myelinated nerve fiber (black asterisk) in an astrocytic process in the hippocampal *stratum alveus*. Bar, 500 nm. (**B**) Astrocytic processes with presumptive multilammelar body (black asterisk), an autophagosomic vesicle variant. Numerous degenerating mitochondria are also evident in this profile (1-6). Bar, 500 nm. (**C**) Perivascular astrocyte in the *stratum pyramidale* exhibiting a hydropic process (Ap) with numerous vacuoles (vac) and swollen mitochondria (1,2). Note the lumen of a nearby capillary (cap). Bar, 500 nm.

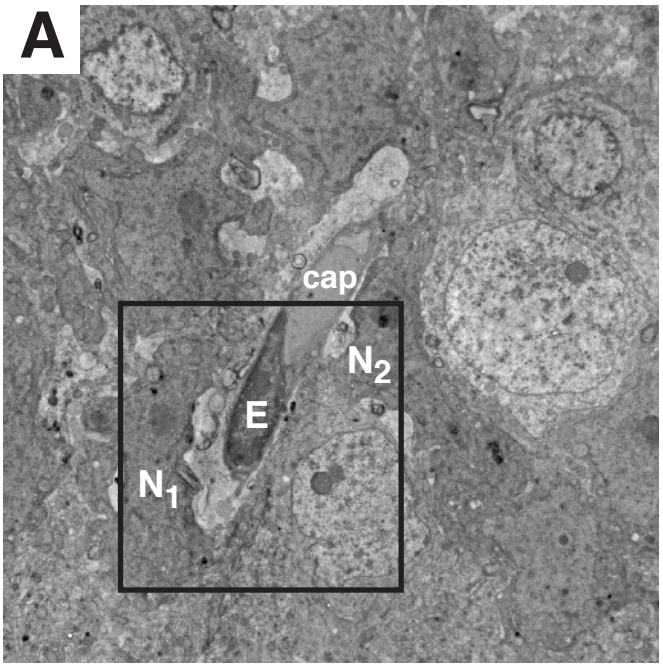

Fig. S20. Degenerating ("dark") pyramidal neurons in the hippocampus CA1 stratum pyramidale in a C57BL/6 mouse brain two weeks after exposure to a single shock tube blast. (**A**) "Dark" neurons (N_1,N_2) and adjacent capillary (cap) and endothelial cell (E) in a blast-exposed mouse hippocampus (Fig. 4J). Black box outlines enlarged region in (B) below. (**B**) Degenerating neurons (N_1,N_2) with electron-dense ("dark") cytoplasm and irregularly shaped nuclear envelopes (white arrows). A nearby capillary (cap) and endothelial cell (E) are surrounded by grossly swollen astrocytic end-feet (Af) containing dilated vacuoles (vac). A normal-appearing neuron (N_3) is present in this micrograph. Bar, 2 μm.

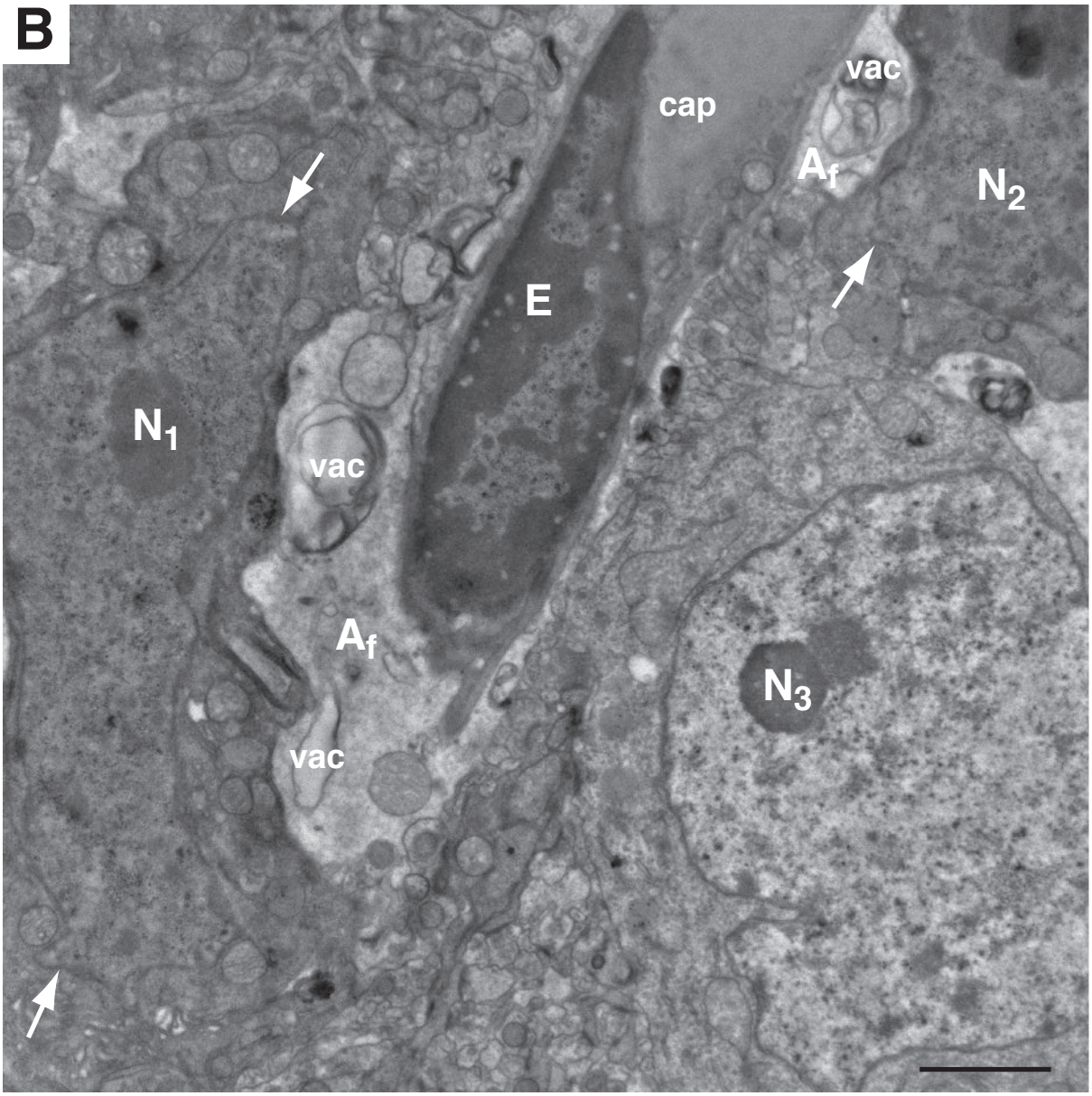

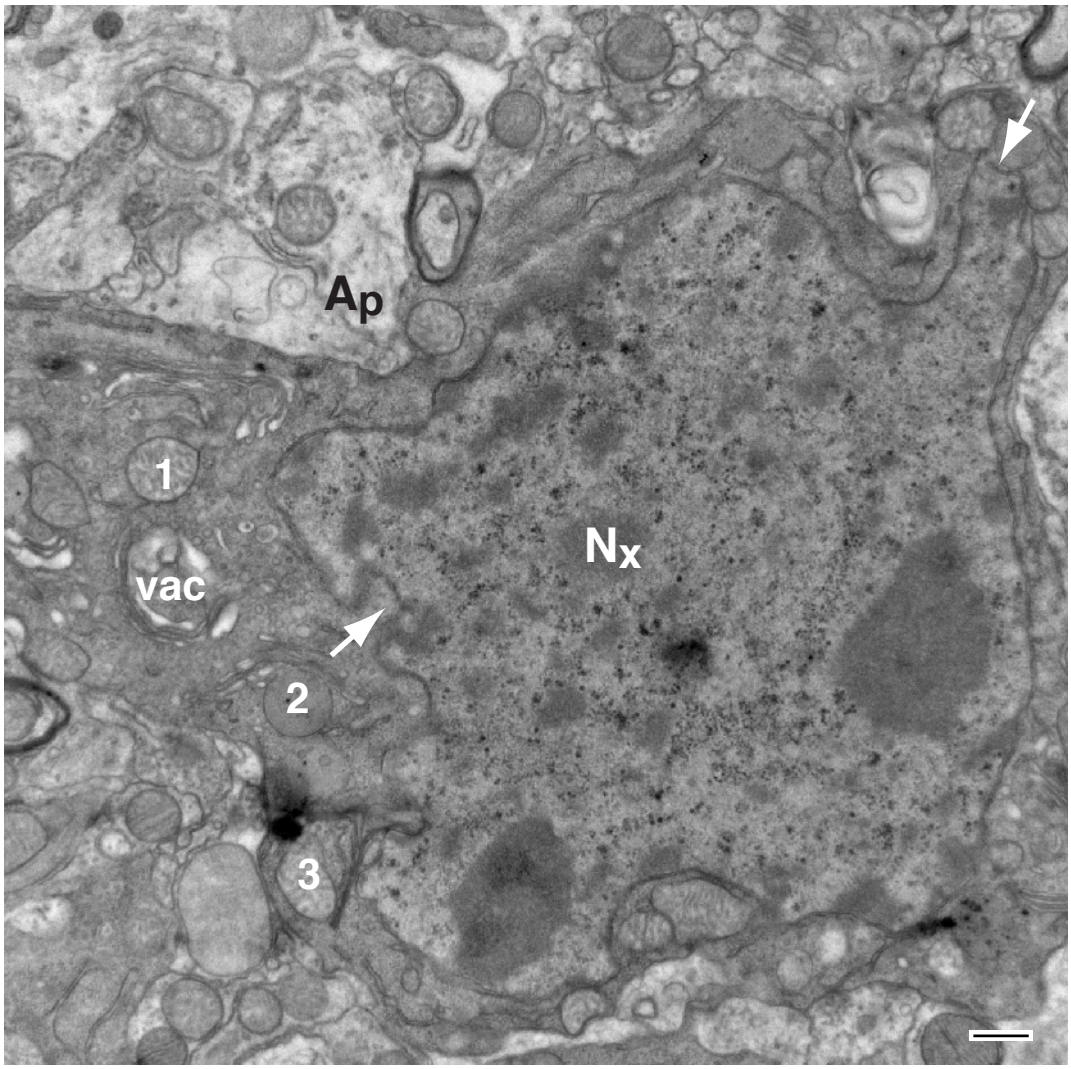

Fig. S21. Degenerating ("dark") pyramidal neurons in the hippocampus CA1 stratum pyramidale in a C57BL/6 mouse brain two weeks after exposure to a single shock tube blast. Degenerating pyramidal neuron (Nx) is characteristically electron-dense ("dark") and exhibits a convoluted nuclear envelope (white arrows). Vacuoles (vac) and degenerating mitochondria (numbers 1-4) are also present. An adjacent hydropic astrocytic process (Ap) is also evident in this micrograph. Bar, 500 nm.

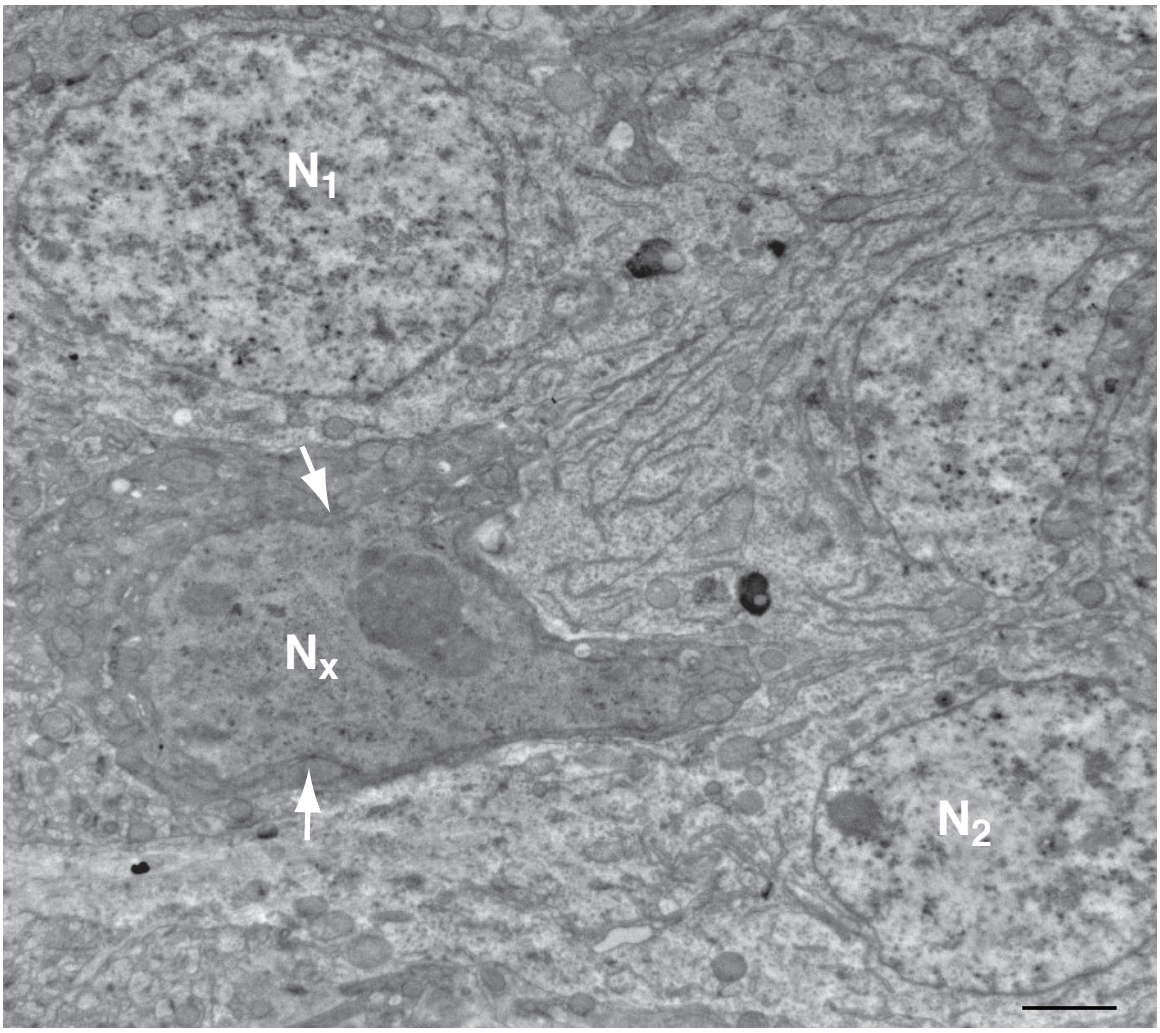

Fig. S22. Degenerating ("dark") pyramidal neurons in the hippocampus CA1 stratum pyramidale in a C57BL/6 mouse brain two weeks after exposure to a single shock tube blast. A degenerating pyramidal neuron (Nx) exhibits electron-dense ("dark") cytoplasm and comparably electron-dense nucleus with an irregularly contoured nuclear envelope (white arrows). "Dark" neurons correspond to the pyknotic pyramidal neurons observed in adjacent toluidine blue-stained semi-thick section (Fig. 4H). Two neighboring pyramidal neurons (N_1, N_2) demonstrate relatively normal ultrastructure. Bar, 2 μm.

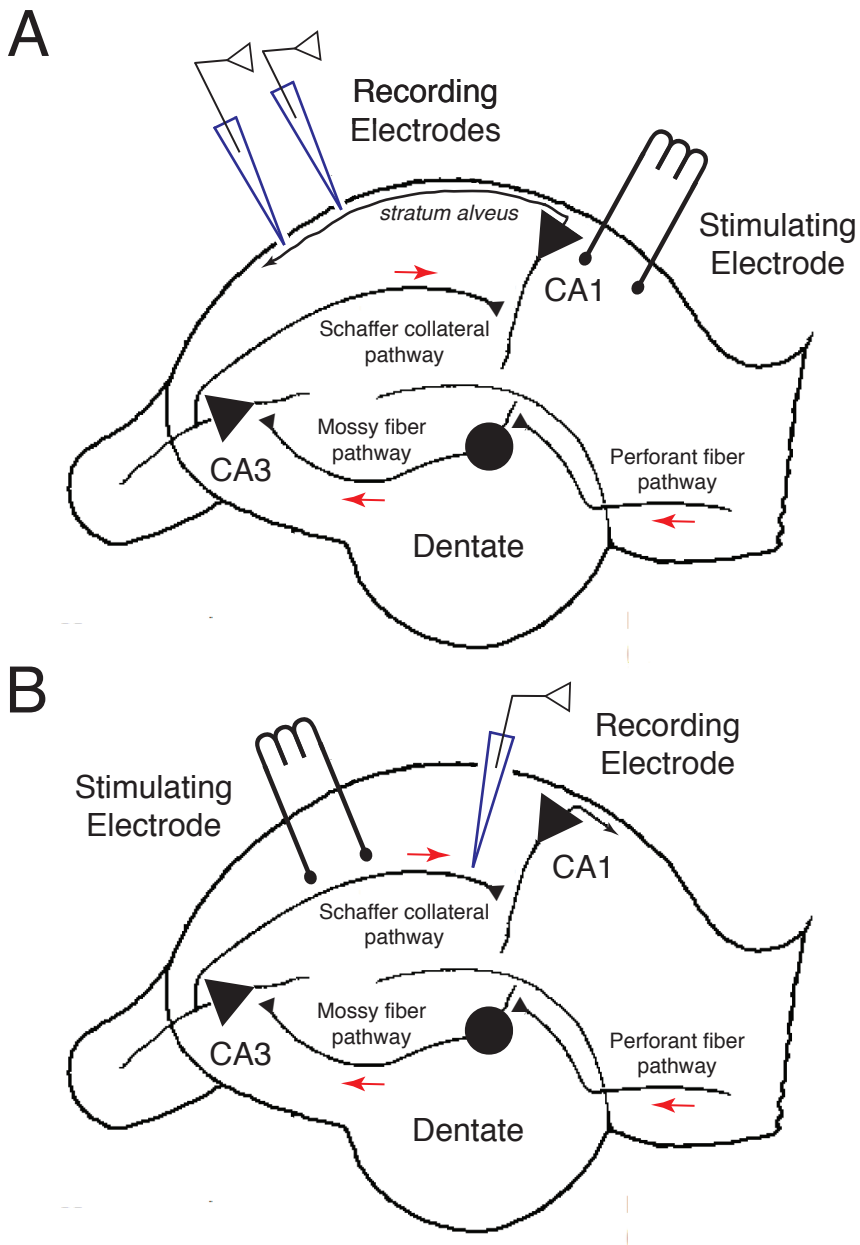

Fig. S23. Electrode placements for axonal conduction velocity and synaptic plasticity experiments. (**A**) Schematic of the hippocampal slice preparation illustrating electrophysiological arrangement for evaluating axonal conduction velocity in the *stratum alveus*, the hippocampal CA1 axonal output pathway. The positioning of a stimulating electrode and two recording electrodes in *stratum alveus* of field CA1 are shown relative to local Schaffer collateral-CA1 synaptic circuitry. Recordings of compound action potentials from CA1 pyramidal neurons were used to calculate axonal conduction velocity in the *stratum alveus*. The time difference between peak negativities at the two recording sites illustrated by each arrow in the CA1 axonal output pathway and distance between the electrodes was used to calculate conduction velocity. (**B**) Schematic of the hippocampal slice preparation illustrating positioning of stimulation and recording electrodes in *stratum radiatum* of field CA1 to record Schaffer collateral-evoked field excitatory postsynaptic potentials (fEPSPs) to measure stimulus-evoked and chemically-evoked cAMP-dependent long-term potentiation (LTP) of Schaffer collateral-CA1 synaptic transmission. See *Methods* for details.

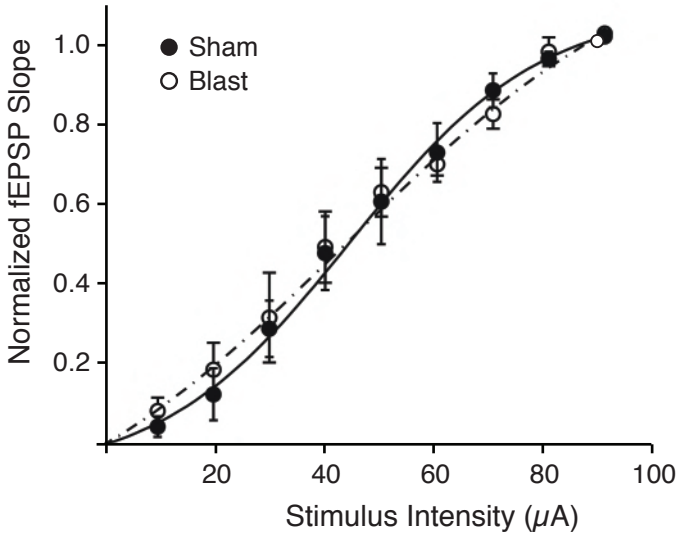

Fig. S24. Schaffer collateral-CA1 synaptic input-output relations illustrating the absence of long-term effects of blast exposure on *baseline* synaptic transmission. Hippocampal slices were prepared from mice exposed to a single blast (○) compared to control sham-blast (●) four weeks after experimental exposure. Normalized peak fEPSP slope amplitudes are plotted versus Schaffer collateral stimulus intensity. The curves demonstrate that a given intensity of synaptic stimulation elicited the same magnitude response in hippocampal slices from blast-exposed mice compared to sham-blast controls.

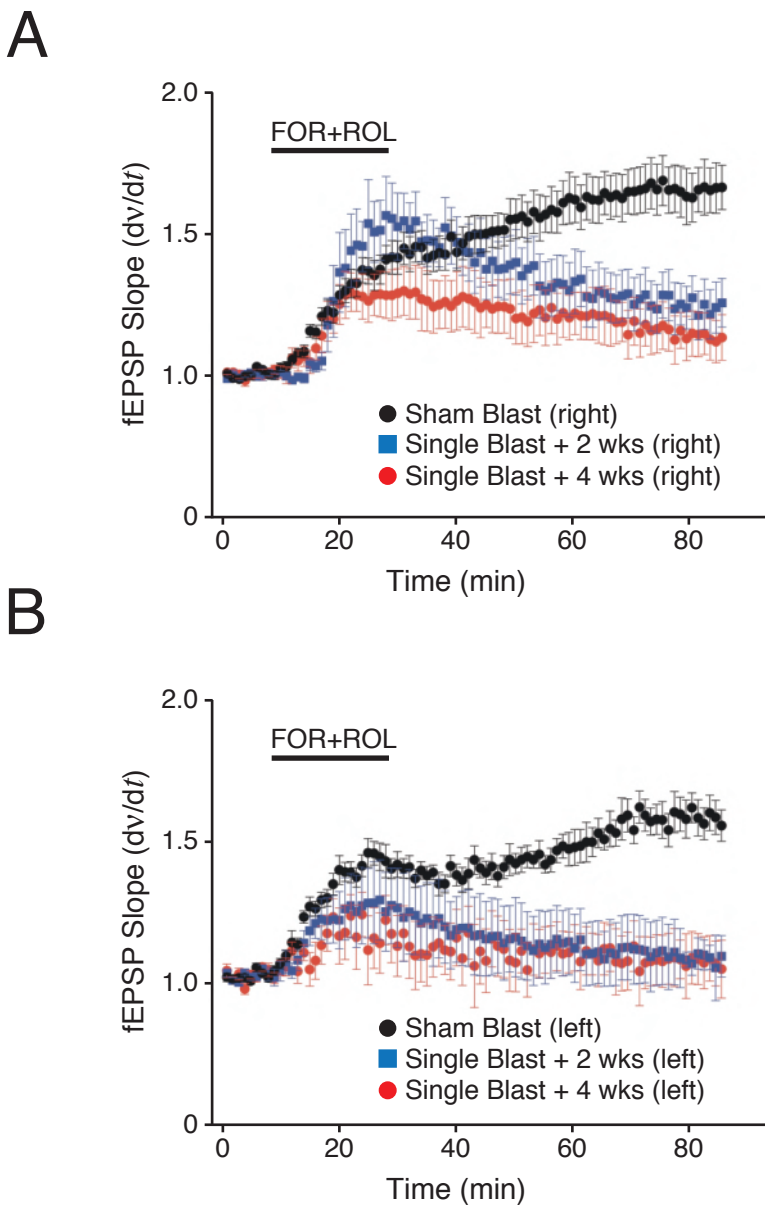

Fig. S25. Blast-induced deficits in cAMP-induced long-term potentiation of synaptic transmission at Schaffer collateral-CA1 synapses are bilateral and persistent.
(**A**) Time course of cyclic AMP-induced LTP evoked by bath application of the adenylate cyclase activator forskolin (50μM) plus the type II phosphodiesterase inhibitor rolipram (10μM) (FOR+ROL; solid bar) in hippocampal slices from the right hemisphere from mice exposed to a single shock tube blast two weeks (■, n=6) or four weeks (●, n=9) before sacrifice compared to sham-blast control mice (●, n=10). (**B**) Time course of cyclic AMP-induced LTP evoked by bath application of the adenylate cyclase activator forskolin (50μM) plus the type II phosphodiesterase inhibitor rolipram (10μM) (FOR+ROL; solid bar) in hippocampal slices from the left hemisphere from mice exposed to a single sublethal blast two weeks (■, n=6) or four weeks (●, n=6) before sacrifice compared to sham-blast control mice (●, n=9). Each fEPSP point = mean ± S.E.M..

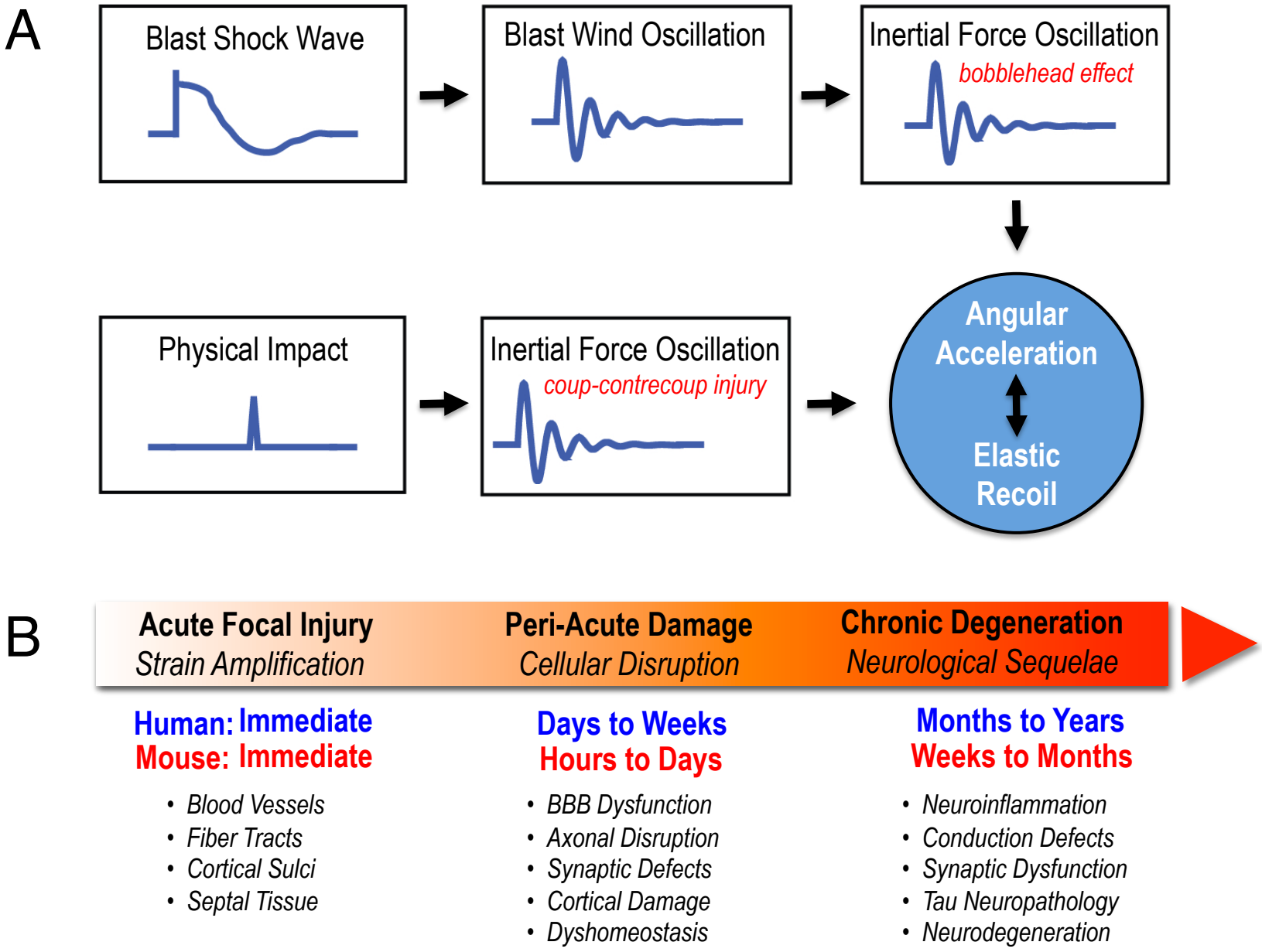

Fig. S26. Model of blast- and concussion-related TBI and sequelae, including CTE.

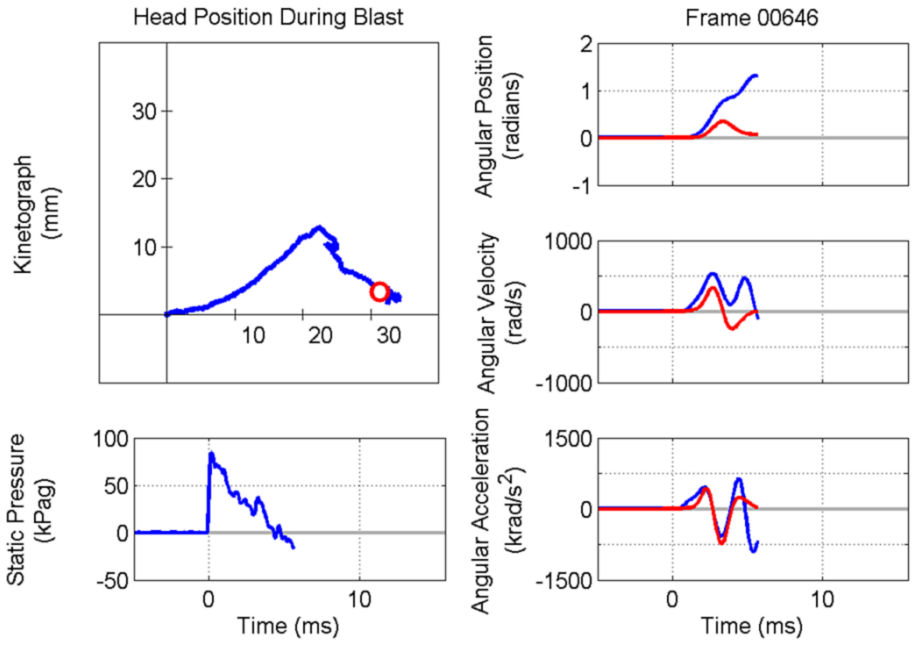

Video S1. Mouse head kinematics during exposure to a single shock tube blast.
Single frame from high-speed videographic kinetograph shows the parametric plot of nose position (top left) during blast exposure as a function of time. Nose position was measured in two directions in which the x-axis is parallel to the axis of the shock tube and the y-axis is perpendicular to ground. High-speed videographic record of the blast pressure waveform (bottom left) shows a plot of the coincident free-field pressure dynamics as a function of time. On the right, the radial kinematics, position, velocity and acceleration of blast-induced head movement in both the horizontal (blue) and sagittal (red) planes are shown as a function of time. Static pressure data was processed with 2 kHz low-pass filtering. Angular position data was processed with 500 Hz low-pass filtering.*The complete Supplemental Video S1 is available as a downloadable avi-formatted video file.*